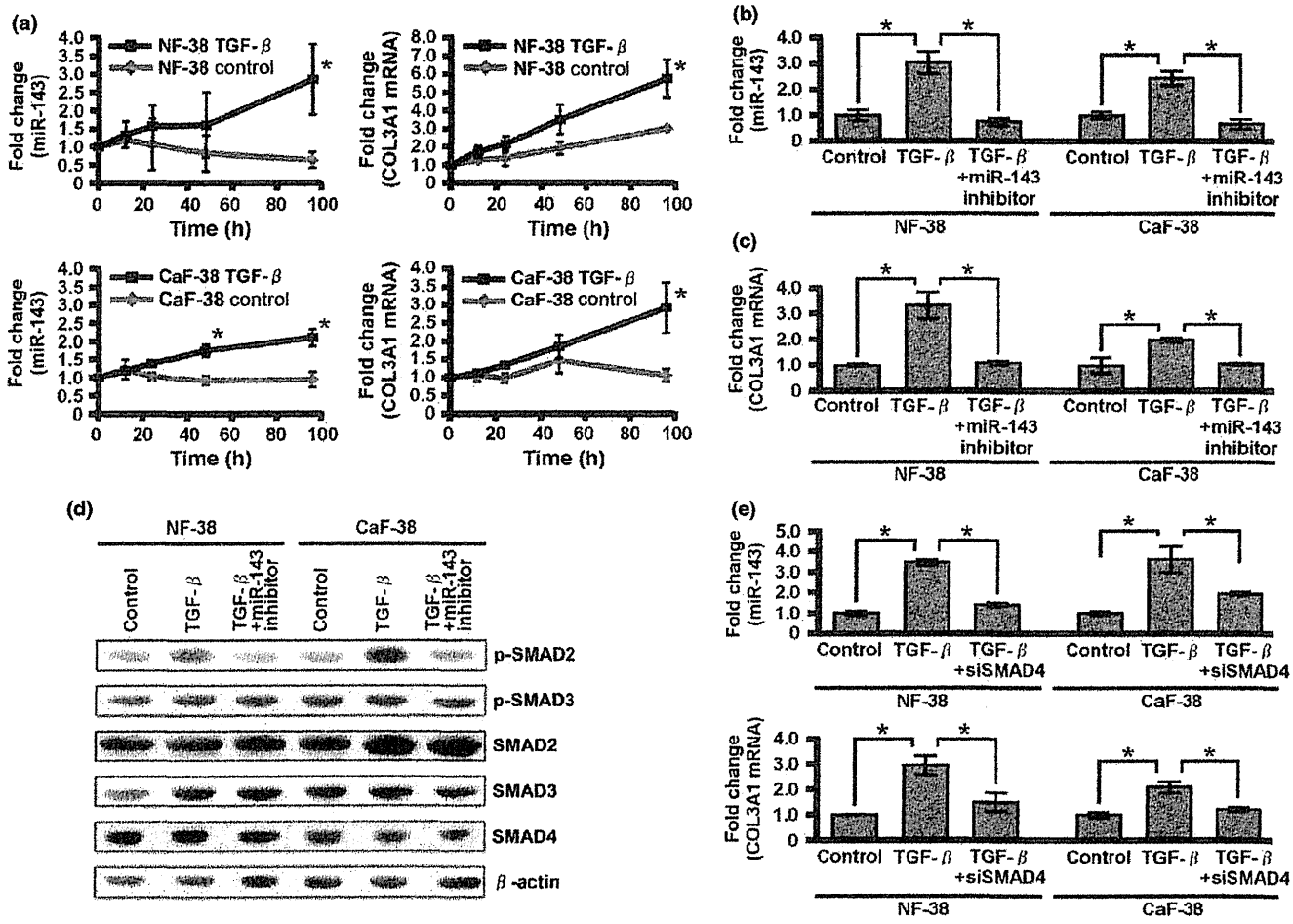

Fig. 4. Effect of transforming growth factor-β (TGF-β) on microRNA-143 (miR-143) and collagen type III expression. (a) Quantitative RT-PCR analysis of miR-143 and collagen type III mRNA in normal gastric fibroblasts (NF-38) and cancer-associated fibroblasts (CaF-38) after the indicated times of TGF-β1 treatment. (b) MicroRNA-143 expression levels in NF-38 and CaF-38 in the absence or presence of TGF-β1 with or without miR-143 inhibitor. (c) Collagen type III mRNA expression levels in NF-38 and CaF-38 in the absence or presence of TGF-β with or without miR-143 inhibitor. (d) Expression levels of TGF-β family signal components were determined by Western blot analysis. (e) Quantitative RT-PCR analysis of miR-143 and collagen type III mRNA in NF-38 and CaF-38 with *SMAD4* siRNA. Results are mean ± SE of triplicate measurements. $^*P < 0.05$.

both fibroblasts (Fig. 4a). However, the induction of collagen type III mRNA in fibroblasts by TGF-β1 was significantly suppressed by pretreatment with miR-143 inhibitor (Fig. 4b,c). Interestingly, miR-143 inhibitor significantly suppressed the expression of p-SMAD2 (Fig. 4d), and *SMAD4* siRNA significantly downregulated miR-143 and collagen type III mRNA expression in each fibroblast (Fig. 4e). These data imply that miR-143 is deeply involved in the regulation of collagen type III expression by TGF-β/SMAD signaling in NF and CaF.

Correlation between miR-143 expression and clinicopathological characteristics of GC. To investigate the relation between miR-143 expression and clinicopathological parameters, we examined miR-143 expression levels in 68 formalin-fixed paraffin-embedded samples of primary GC by qRT-PCR. The

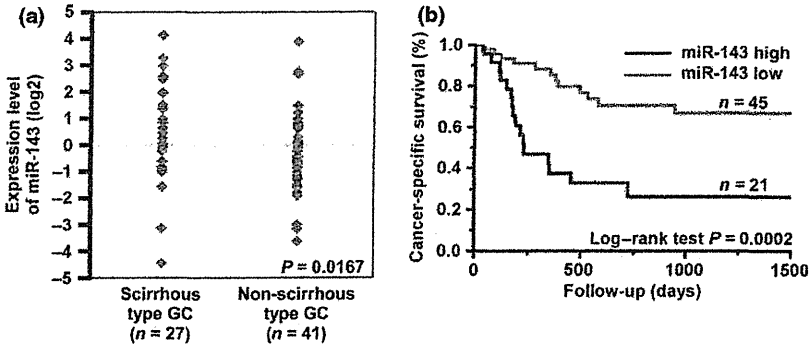

Fig. 5. Relation between microRNA-143 (miR-143) expression and patient prognosis. (a) Expression levels of miR-143 in formalin-fixed paraffin-embedded gastric cancer (GC) tissue samples ($n = 68$) were measured by quantitative RT-PCR analysis. (b) Cancer-specific survival of 68 patients with GC based on expression levels of miR-143 was examined. The expression levels of miR-143 were divided into two groups, high and low expression of miR-143, based on one-third of the miR-143 expression level (cut-off line = one-third of miR-143 expression level in this group).

Table 2. Relationship between microRNA-143 (miR-143) expression and clinicopathological characteristics in 68 patients with gastric cancer

	miR-143 expression		*P*-value†
	High (%)	Low	
Age, years			
<60	7 (25.9)	20	0.2640
≥60	16 (39.0)	25	
Sex			
Male	14 (29.2)	34	0.2086
Female	9 (45.0)	11	
Stage			
I/II	3 (11.1)	24	0.0013
III/IV	20 (48.8)	21	
Histological classification			
Well differentiated	8 (27.6)	21	0.3485
Poorly differentiated	15 (38.5)	24	
Non-scirrhous	10 (24.4)	31	0.0428
Scirrhous	13 (48.1)	14	

†Fisher's exact test.

Table 3. Univariate and multivariate analysis of factors influencing survival in 68 patients with gastric cancer

	Univariate analysis		Multivariate analysis	
	HR (95% CI)	*P*-value	HR (95% CI)	*P*-value
Age, years				
<60	1 (Ref.)	0.4585		
≥60	1.34 (0.63–3.01)			
Sex				
Female	1 (Ref.)	0.4116		
Male	1.18 (0.78–1.72)			
Stage				
I/II	1 (Ref.)	<0.0001	1 (Ref.)	0.0004
III/IV	7.95 (2.78–33.47)		6.20 (2.10–26.52)	
Histological type				
Well differentiated	1 (Ref.)	0.9513		
Poorly differentiated	0.98 (0.46–2.11)			
Non-scirrhous	1 (Ref.)	0.1435		
Scirrhous	1.75 (0.82–3.70)			
Expression of miR-143				
Low	1 (Ref.)	0.0005	1 (Ref.)	0.0141
High	3.81 (1.80–8.29)		2.62 (1.21–5.80)	

CI, confidence interval; HR, hazard ratio; miR-143, microRNA-143; Ref., reference.

miR-143 expression levels were significantly higher in scirrhous type GC cases than in non-scirrhous type GC cases ($P = 0.0167$; Fig. 5a). As shown in Table 2, miR-143-positive GC cases showed advanced tumor stage ($P = 0.0013$) and tended to have scirrhous type histology ($P = 0.0428$) in comparison with miR-143-negative cases. Kaplan–Meier analysis showed that GC patients with high miR-143 expression correlated significantly with worse cancer-specific mortality ($P = 0.0002$, log–rank test; Fig. 5b). When limited to the cases with scirrhous type GC or non-scirrhous type GC, miR-143 expression had no prognostic effect (data not shown). Univariate and multivariate analysis showed miR-143 to be an independent prognostic marker of GC cases ($P = 0.0141$; Table 3).

DNA methylation may suppress miR-143 expression, which regulates scirrhous type GC cell invasion. Expression of miR-143 was detected in epithelial cells of non-neoplastic tissue, but its expression was suppressed in cancer cells (Fig. 2). To pursue the cause of miR-143 suppression in GC cell lines, we treated MKN-1 and HSC-44PE cell lines with 0–3 μmol/L 5-aza-2′-deoxycytidine for 4 days and analyzed sequential changes in miR-143 expression by qRT-PCR. Expression of miR-143 was restored by 5-aza-2′-deoxycytidine treatments (Fig. S3a), suggesting that DNA methylation may cause transcriptional inactivation of miR-143 in GC cells.

Next, to confirm the possible antiproliferative or anti-invasive effects of miR-143 on cancer cells, MTT and Transwell invasion assays were carried out using MKN-1 and HSC-44PE GC cell lines with forced miR-143 expression by miR-143 precursor transfection. Cell growth of each GC cell line with forced miR-143 expression did not differ from that of cells transfected with control miRNA (data not shown). However, the invasiveness of cell lines with miR-143 forced expression was reduced compared to that of the negative control miRNA-transfected cell lines (Fig. S3b). These data verified that exogenous recovery of miR-143 expression could suppress the invasiveness of cancer cells but not the proliferative activity.

Discussion

We report here that miR-143 expression was conserved in scirrhous type GC tissues and that the main source of miR-143 was stromal fibroblasts. MicroRNA-143 could regulate TGF-β /SMAD signaling to mediate the expression of collagen type III in stromal fibroblast of scirrhous type GC. We further showed that miR-143 maintenance or overexpression was significantly associated with advanced stage and poor clinical survival in GC. To our knowledge, this is the first report that refers to the importance of miR-143 in stromal fibroblasts of cancer.

Cancer cells and stromal fibroblasts interact with each other through various growth factors.[5] Among such growth factors, TGF-β signaling plays an important role in progression of scirrhous type GC.[5] It has been reported that some miRNAs regulate tissue fibrosis in various organs.[35–38] In the present study, we have identified a novel role for miR-143 in the regulation of collagen type III expression. Although TGF-β treatment induced collagen type III mRNA expression, downregulation of miR-143 expression significantly suppressed the induction of collagen type III in fibroblasts. The classic TGF-β signaling pathway involves the SMAD protein family.[39] The SMAD-dependent regulation of collagens by TGF-β has well-established mechanisms,[40–43] and collagen type III transcription is targeted by SMAD3.[40,42] The induction of collagen type III in gastric fibroblasts could be regulated by the same mechanism because *SMAD4* siRNA could inhibit collagen type III expression in NFs and CaFs. Although we detected that miR-143 only affected the activation of SMAD2, the expression of p-SMAD3 seemed to be high enough for the regulation of collagen type III expression. It is well known that both p-SMAD2 and p-SMAD3 are essential for forming com-

plexes with SMAD4, and this complex is crucial for activation of TGF-β/SMAD signaling.[39] Taken together, it could be speculated that activation of SMAD2, regulated by miR-143, is a trigger for enhancing collagen type III expression in NFs and CaFs. It has been generally accepted that miRNAs repress the translation of their targets.[44,45] Based on present results, it could be suspected that miR-143 regulates collagen type III expression by targeting some inhibitor of TGF-β/SMAD2 signaling. Further investigations are required to elucidate the underlying mechanism of collagen type III regulation by miR-143 in cancer stromal fibroblasts.

It has been reported that miR-143 acts as a tumor suppressor gene, and its downregulation is correlated with worse patient outcome.[20,46] However, these previous reports focused on the role of miR-143 in cancer cells and normal cells, and the function of miR-143 in stromal cells surrounding tumor cells has not been discussed. In the present study, we suggest that promoter hypermethylation is involved in downregulation of miR-143 expression in cancer cells. In addition, forced expression of miR-143 in GC cell lines significantly inhibited their invasiveness. Taken together, there is very strong evidence that the tumor suppressive role of miR-143 is downregulated by promoter hypermethylation in cancer cells. However, we also showed that miR-143 expression was localized within stromal fibroblasts, but not in cancer cells in scirrhous type GC, and contributed to the regulation of collagen type III expression and cancer cell proliferation. We also showed that miR-143 expression was higher in scirrhous type GC than in non-scirrhous type GC. In addition, its expression correlated significantly with advanced pathological stage and poor patient prognosis. Stromal fibrosis in cancer leads to increased matrix rigidity and subsequent activation of cancer cell proliferation through integrin-MAPK signaling.[11] It is common knowledge that fibrosis in cancer tissue can also lead to an increase in interstitial pressure that inhibits efficient drug delivery, resulting in chemoresistance.[8–10] Taken together, miR-143 expression in stromal fibroblasts of scirrhous type GC may participate in cancer progression and lead to poor clinical outcome.

In conclusion, our data position miR-143 as a critical mediator of collagen type III expression in scirrhous type GC. Consequently, miR-143 in cancer stroma may support the progression of scirrhous type GC through fibrillar formation, consistent with the effect of certain oncogenes. Full elucidation of the molecular mechanisms of miR-143 in stromal fibroblasts surrounding cancer cells may improve our understanding of tumor progression in scirrhous type GC.

Acknowledgments

We thank Mr. Shinichi Norimura for excellent technical assistance. This work was carried out with the kind cooperation of the Research Center for Molecular Medicine, Faculty of Medicine, Hiroshima University (Hiroshima, Japan). We thank the Analysis Center of Life Science, Hiroshima University, for the use of their facilities. This work was supported by Grants-in-Aid for Research from the Ministry of Education, Culture, Science, Sports, and Technology of Japan, and, in part, by a Grant-in-Aid for the Third Comprehensive 10-Year Strategy for Cancer Control and for Cancer Research from the Ministry of Health, Labour and Welfare of Japan, and by The National Institute of Biomedical Innovation (Program for Promotion of Fundamental Studies in Health Sciences). This work was also supported in part by a Research Fellowship from the Japan Society for the Promotion of Science and the National Cancer Center Research and Development Fund (23-A-9).

Disclosure Statement

The authors have no conflict of interest.

References

1 Hohenberger P, Gretschel S. Gastric cancer. *Lancet* 2003; **362**: 305–15.
2 Lauren P. The two histological main types of gastric carcinoma: diffuse and so-called intestinal-type carcinoma. an attempt at a histo-clinical classification. *Acta Pathol Microbiol Scand* 1965; **64**: 31–49.
3 Otsuji E, Kuriu Y, Okamoto K *et al.* Outcome of surgical treatment for patients with scirrhous carcinoma of the stomach. *Am J Surg* 2004; **188**: 327–32.
4 Ikeguchi M, Miyake T, Matsunaga T *et al.* Recent results of therapy for scirrhous gastric cancer. *Surg Today* 2009; **39**: 290–4.
5 Yashiro M, Hirakawa K. Cancer-stromal interactions in scirrhous gastric carcinoma. *Cancer Microenviron* 2010; **3**: 127–35.
6 Yamamoto M, Sumiyoshi H, Nakagami K, Taniyama K, Tahara E. Distribution of collagen types I and III and basal lamina in human gastric carcinoma: an immunohistochemical and electron microscopic study. *Virchows Arch A Pathol Anat Histopathol* 1984; **403**: 313–22.
7 Yoshida K, Yokozaki H, Niimoto M, Ito H, Ito M, Tahara E. Expression of TGF-beta and procollagen type I and type III in human gastric carcinomas. *Int J Cancer* 1989; **44**: 394–8.
8 Jain RK. Barriers to drug delivery in solid tumors. *Sci Am* 1994; **271**: 58–65.
9 Heldin CH, Rubin K, Pietras K, Ostman A. High interstitial fluid pressure – an obstacle in cancer therapy. *Nat Rev Cancer* 2004; **4**: 806–13.
10 Nakajima TE, Yanagihara K, Takigahira M *et al.* Antitumor effect of SN-38-releasing polymeric micelles, NK012, on spontaneous peritoneal metastases from orthotopic gastric cancer in mice compared with irinotecan. *Cancer Res* 2008; **68**: 9318–22.
11 Worthley DL, Giraud AS, Wang TC. The extracellular matrix in digestive cancer. *Cancer Microenviron* 2010; **3**: 177–85.
12 Bartel DP. MicroRNAs: genomics, biogenesis, mechanism, and function. *Cell* 2004; **116**: 281–97.
13 Ambros V. The functions of animal microRNAs. *Nature* 2004; **431**: 350–5.
14 Calin GA, Croce CM. MicroRNA signatures in human cancers. *Nat Rev Cancer* 2006; **6**: 857–66.
15 Li X, Luo F, Li Q *et al.* Identification of new aberrantly expressed miRNAs in intestinal-type gastric cancer and its clinical significance. *Oncol Rep* 2011; **26**: 1431–9.
16 Ueda T, Volinia S, Okumura H *et al.* Relation between microRNA expression and progression and prognosis of gastric cancer: a microRNA expression analysis. *Lancet Oncol* 2010; **11**: 136–46.
17 Takei Y, Takigahira M, Mihara K, Tarumi Y, Yanagihara K. The metastasis-associated microRNA miR-516a-3p is a novel therapeutic target for inhibiting peritoneal dissemination of human scirrhous gastric cancer. *Cancer Res* 2011; **71**: 1442–53.
18 Long X, Miano JM. Transforming growth factor-β1 (TGF-β1) utilized distinct pathways for the transcriptional activation of microRNA 143/145 in human coronary artery smooth muscle cells. *J Biol Chem* 2011; **286**: 30119–29.
19 Chen X, Guo X, Zhang H *et al.* Role of miR-143 targeting KRAS in colorectal tumorigenesis. *Oncogene* 2009; **28**: 1385–92.
20 Dou L, Zheng D, Li J *et al.* Methylation-mediated repression of microRNA-143 enhances MLL-AF4 oncogene expression. *Oncogene* 2012; **31**: 507–17.
21 Pagliuca A, Valvo C, Fabrizi E *et al.* Analysis of the combined action of miR-143 and miR-145 on oncogenic pathways in colorectal cancer cells reveals a coordinate program of gene repression. *Oncogene* 2012; **5**: 495.
22 Noguchi S, Yasui Y, Iwasaki J *et al.* Replacement treatment with microRNA-143 and -145 induces synergistic inhibition of the growth of human bladder cancer cells by regulating PI3K/Akt and MAPK signaling pathways. *Cancer Lett* 2013; **328**: 353–61.
23 Fuyuhiro Y, Yashiro M, Noda S *et al.* Cancer-associated orthotopic myofibroblasts stimulates the motility of gastric carcinoma cells. *Cancer Sci* 2012; **103**: 797–805.
24 Naito Y, Oue N, Hinoi T *et al.* Reg IV is a direct target of intestinal transcriptional factor CDX2 in gastric cancer. *PLoS ONE* 2012; **7**: e47545.
25 Yasui W, Ayhan A, Kitadai Y *et al.* Increased expression of p34cdc2 and its kinase activity in human gastric and colonic carcinomas. *Int J Cancer* 1993; **53**: 36–41.

26 Nuovo GJ, Elton TS, Nana-Sinkam P, Volinia S, Croce CM, Schmittgen TD. A methodology for the combined in situ analyses of the precursor and mature forms of microRNAs and correlation with their putative targets. *Nat Protoc* 2009; **4**: 107–15.
27 Alley MC, Scudiero DA, Monks A *et al.* Feasibility of drug screening with panels of human tumor cell lines using a microculture tetrazolium assay. *Cancer Res* 1988; **48**: 589–601.
28 Sentani K, Oue N, Naito Y *et al.* Upregulation of HOXA10 in gastric cancer with the intestinal mucin phenotype: reduction during tumor progression and favorable prognosis. *Carcinogenesis* 2012; **33**: 1081–8.
29 Takagi T, Iio A, Nakagawa Y, Naoe T, Tanigawa N, Akao Y. Decreased expression of microRNA-143 and -145 in human gastric cancers. *Oncology* 2009; **77**: 12–21.
30 Kalluri R, Zeisberg M. Fibroblasts in cancer. *Nat Rev Cancer* 2006; **6**: 392–401.
31 Niitsu Y, Ito N, Kohda K *et al.* Immunohistochemical identification of type I procollagen in tumour cells of scirrhous adenocarcinoma of the stomach. *Br J Cancer* 1988; **57**: 79–82.
32 Mahara K, Kato J, Terui T *et al.* Transforming growth factor beta 1 secreted from scirrhous gastric cancer cells is associated with excess collagen deposition in the tissue. *Br J Cancer* 1994; **69**: 777–83.
33 Kawajiri H, Yashiro M, Shinto O *et al.* A novel transforming growth factor beta receptor kinase inhibitor, A-77, prevents the peritoneal dissemination of scirrhous gastric carcinoma. *Clin Cancer Res* 2008; **14**: 2850–60.
34 Shinto O, Yashiro M, Kawajiri H *et al.* Inhibitory effect of a TGFbeta receptor type-I inhibitor, Ki26894, on invasiveness of scirrhous gastric cancer cells. *Br J Cancer* 2010; **102**: 844–51.
35 Chung AC, Huang XR, Meng X, Lan HY. miR-192 mediates TGF-beta/Smad3-driven renal fibrosis. *J Am Soc Nephrol* 2010; **21**: 1317–25.
36 Qin W, Chung AC, Huang XR *et al.* TGF-beta/Smad3 signaling promotes renal fibrosis by inhibiting miR-29. *J Am Soc Nephrol* 2011; **22**: 1462–74.
37 Honda N, Jinnin M, Kajihara I *et al.* TGF-beta-mediated downregulation of microRNA-196a contributes to the constitutive upregulated type I collagen expression in scleroderma dermal fibroblasts. *J Immunol* 2012; **188**: 3323–31.
38 Yang S, Cui H, Xie N *et al.* miR-145 regulates myofibroblast differentiation and lung fibrosis. *FASEB J* 2013; **27**: 2382–91.
39 Derynck R, Zhang YE. Smad-dependent and Smad-independent pathways in TGF-beta family signalling. *Nature* 2003; **425**: 577–84.
40 Verrecchia F, Chu ML, Mauviel A. Identification of novel TGF-beta/Smad gene targets in dermal fibroblasts using a combined cDNA microarray/promoter transactivation approach. *J Biol Chem* 2001; **276**: 17058–62.
41 Verrecchia F, Mauviel A, Farge D. Transforming growth factor-beta signaling through the Smad proteins: role in systemic sclerosis. *Autoimmun Rev* 2006; **5**: 563–9.
42 Kim HJ, Kim MY, Jin H *et al.* Peroxisome proliferator-activated receptor delta regulates extracellular matrix and apoptosis of vascular smooth muscle cells through the activation of transforming growth factor-{beta}1/Smad3. *Circ Res* 2009; **105**: 16–24.
43 Zong L, Qu Y, Xu MY, Dong YW, Lu LG. 18alpha-glycyrrhetinic acid down-regulates expression of type I and III collagen via TGF-Beta1/Smad signaling pathway in human and rat hepatic stellate cells. *Int J Med Sci* 2012; **9**: 370–9.
44 Esquela-Kerscher A, Slack FJ. Oncomirs – microRNAs with a role in cancer. *Nat Rev Cancer* 2006; **6**: 259–69.
45 Iorio MV, Croce CM. microRNA involvement in human cancer. *Carcinogenesis* 2012; **33**: 1126–33.
46 Liu R, Liao J, Yang M *et al.* The cluster of miR-143 and miR-145 affects the risk for esophageal squamous cell carcinoma through co-regulating fascin homolog 1. *PLoS ONE* 2013; **7**: e33987.

Supporting Information

Additional supporting information may be found in the online version of this article:

Fig. S1. α-Smooth muscle actin mRNA expression in normal gastric fibroblasts and cancer-associated fibroblasts.

Fig. S2. Transforming growth factor-β expression in normal gastric fibroblasts and cancer-associated fibroblasts.

Fig. S3. MicroRNA-143 expression might be suppressed by DNA methylation and effects on cell invasion of gastric cancer cell lines.

Table S1. Information on fibroblasts.

Data S1. Supplementary materials and methods.

Cancer Science
Japanese Cancer Association JCA
Open Access

MicroRNA-148a is downregulated in gastric cancer, targets MMP7, and indicates tumor invasiveness and poor prognosis

Naoya Sakamoto,[1] Yutaka Naito,[1] Naohide Oue,[1] Kazuhiro Sentani,[1] Naohiro Uraoka,[1] Htoo Zarni Oo,[1] Kazuyoshi Yanagihara,[2] Kazuhiko Aoyagi,[3] Hiroki Sasaki[3] and Wataru Yasui[1]

[1]Department of Molecular Pathology, Hiroshima University Institute of Biomedical and Health Sciences, Hiroshima; [2]Division of Translational Research, Exploratory Oncology and Clinical Trial Center, National Cancer Center, Chiba; [3]Division of Genetics, National Cancer Center Research Institute, Tokyo, Japan

Key words
Gastric cancer, microRNA, miR-148a, MMP7, cancer invasion

Correspondence
Wataru Yasui, Department of Molecular Pathology, Hiroshima University Institute of Biomedical and Health Sciences, 1-2-3 Kasumi, Minami-ku, Hiroshima 734-8551, Japan.
Tel: +81-82-257-5145; Fax: +81-82-257-5149;
E-mail: wyasui@hiroshima-u.ac.jp

Funding Information
Ministry of Education, Culture, Science, Sports, and Technology of Japan. Ministry of Health, Labor and Welfare of Japan. The National Institute of Biomedical Innovation. The Japan Society for the Promotion of Science. The National Cancer Center Research and Development Fund.

Received August 20, 2013; Revised November 16, 2013; Accepted November 26, 2013

Cancer Sci **105** (2014) 236–243

doi: 10.1111/cas.12330

Gastric cancer (GC) develops through deregulation of gene expression and accumulation of epigenetic abnormalities, leading to tumor cell acquisition of malignant features. MicroRNAs (miRNAs) play a critical role in cancer development where they can act as oncogenes or oncosuppressors. To identify miRNAs that are associated with some clinicopathologic features of GC and/or participate in tumor progression, miRNA expression in 20 GC tissues and five corresponding non-neoplastic gastric mucosa was examined by miRNA microarray. Oligonucleotide array analysis was carried out for miRNA target prediction. The functions of candidate miRNAs and their target genes were also analyzed by quantitative RT-PCR, Western blotting, reporter gene assay, and cell invasion assay. Comparison of miRNA expression profiles revealed that downregulation of miR-148a was identified in most of the GC tissues. Downregulation of miR-148a was significantly correlated with an advanced clinical stage, lymph node metastasis, and poor clinical outcome. Custom oligonucleotide array analysis revealed that *MMP7* expression was markedly downregulated in miR-148a-overexpressing GC cells; MMP7 was found to be a direct and functional target of miR-148a, participating in cell invasion. These results suggest that miR-148a contributes to the maintenance of homeostasis in normal stomach tissue and plays an important role in GC invasion by regulating MMP7 expression.

Gastric cancer (GC) remains a major public health issue as the fourth most common cancer and the second leading cause of cancer mortality worldwide.[1] Gastric cancer is assumed to originate from a sequential accumulation of molecular and genetic alterations to stomach epithelial cells.[2] A deeper understanding of the pathogenesis and biological features of GC is necessary to further inform and enhance early detection and treatment methods.

MicroRNAs (miRNAs) are non-protein-coding small RNAs in the size range of 19–25 nucleotides, which play important regulatory roles in posttranscriptional repression and fine-tune various essential biological processes.[3–5] Recent data clearly shows that miRNAs are abnormally expressed in various cancers, indicating novel roles as oncogenes or tumor suppressors in different tumor types.[6] Currently, miRNA target-prediction algorithms and publicly available databases are undergoing rapid and dramatic evolution. However, precision and sensitivity of state-of-the-art algorithms were estimated as ~50% and 12%, respectively, when tested against proteomics-supported miRNA targets,[7] highlighting the necessity for mass experimental miRNA target validation.[8] As for GC, although there are several reports of aberrant expression of specific miRNAs, target predictions of identified miRNAs were carried out by several online databases in each study.[9,10] Each new finding of deregulated miRNA in GC and its target gene is a welcome addition to the body of knowledge; however, there is no denying the possibility that genuine targets can be overlooked using online algorithms.

In the present study, we examined miRNA expression in 20 GC cases and five corresponding non-neoplastic gastric mucosa using miRNA microarray. By comparing these expression profiles, we found downregulation of miR-148a in the majority of GC tissues. The correlation between the miR-148a expression level and clinicopathologic parameters of GC was also examined and we identified that lower expression levels of miR-148a correlate with worse clinicopathologic characters. To predict gene targets of miR-148a, we used an oligonucleotide array to generate a list of genes whose expression was deregulated by altered expression of miR-148a, and found that expression of *MMP7* was suppressed by upregulation of miR-148a. It was confirmed that MMP7 was a direct and functional target of miR-148a using quantitative RT-PCR (qRT-PCR), Western blot analysis, and reporter gene assay. We also carried

out target prediction of miR-148a using representative online databases. However, no lists of miR-148a target genes contained *MMP7*, thus validating the reliability of the conventional laboratory-based experimental strategy for miRNA target prediction, by which crucial target genes were detected-genes, which online target prediction could not detect.

Materials and Methods

MicroRNA microarray hybridization. Total RNA was isolated from frozen tissue with Isogene (Nippon Gene, Tokyo, Japan). Short-strand RNA was purified from total RNA with the RNeasy MinElute Cleanup Kit (Qiagen, Hilden, Germany). For the oligonucleotide array we used Genopal-MICH07 DNA chips (Mitsubishi Rayon, Tokyo, Japan) comprising 188 oligonucleotide DNA probes. Details are described in Data S1.

***In situ* hybridization for miR-148a.** Biotin 3′-labeled locked nucleic acid-incorporated miRNA probe (miR-CURY LNA detection probe; Exiqon, Woburn, MA, USA) was used for visualization of miR-148a. Details are described in Data S1.

Cell lines. Nine cell lines derived from human GC were used. All cell lines were maintained as described previously.[11] Details are described in Data S1.

Oligonucleotide array construction, hybridization, detection, and data analysis. The oligonucleotide array, Genopal (Mitsubishi Rayon), was prepared as described previously.[12] Details of oligonucleotide array probes, total RNA isolation, RNA quantification and assessment of integrity, hybridization, detection, and data analysis were carried out as described previously.[13]

Quantitative RT-PCR and Western blot analysis. Quantification of *MMP7* mRNA levels was carried out using real-time fluorescence detection as described previously.[14] For analysis of miR-148a and U6B, expression levels of miR-148a and RNU6B were measured and quantified as described previously.[15] Western blot analysis was carried out as described previously.[16] Details are described in Data S1.

CpG island determination, genomic DNA extraction, and bisulfite genomic DNA sequencing. A 20-kb genomic DNA fragment encompassing the miRNA coding sequences was analyzed with CpG plot software (http://bioweb2.pasteur.fr). We used the parameter values to report a CpG island as described previously.[17] Thermal cycling conditions were as described previously.[18] Methylation status of PCR products were confirmed as described previously.[19] Details are described in Data S1.

Plasmids. For constitutive expression of the *MMP7* gene, commercially available *MMP7* cDNA construct (Invitrogen, Carlsbad, CA, USA) was purchased. pCMV-MIR (Origene, Rockville, MD, USA) was used for constitutive expression of miR-148a. Details are described in Data S1.

Cell transfection. Transfection of cells was carried out with Lipofectamine RNAiMAX Reagent (Invitrogen) according to the manufacturer's instructions. Details are described in Data S1.

Reporter gene assay. Reporter gene assay was carried out as described previously.[20] Details are described in Data S1.

Tissue samples. A total of 81 primary tumor samples were collected from patients diagnosed with GC. Details are described in Data S1.

Cell growth and *in vitro* invasion assay. For the MTT assay, cells were seeded at a density of 2000 cells per well in 96-well plates. Cell growth was monitored after 1, 2, and 4 days by MTT assay.[21] Modified Boyden chamber assays were used to examine invasiveness as described previously.[20]

Statistical methods. Statistical differences between miRNA levels in non-neoplastic gastric mucosa and GC were evaluated using the Mann–Whitney *U*-test and Wilcoxon matched pairs test. The correlation between expression levels of miR-148a and clinicopathologic parameters was analyzed with Fisher's exact test. Univariate and multivariate Cox regression was used to evaluate the associations between clinical covariates and cancer-specific mortality. Hazard ratios and 95% confidence intervals were estimated from Cox proportional hazard models. P-values < 0.05 were considered to be statistically significant.

Results

MicroRNA microarray analysis. To identify GC-related miRNA, we carried out miRNA microarray profiling to compare between 20 cancer tissue and five corresponding non-neoplastic gastric mucosa. Through the comparison between these two profiles, six miRNAs showed significantly higher expression in corresponding non-neoplastic gastric mucosa than in cancer tissue (Table 1). Among six miRNAs, we focused on miR-148a because its expression was most downregulated in GC tissue. Further analysis of the same GC tissues by qRT-PCR also showed a significant downregulation of miR-148a (Fig. S1).

Clinicopathologic characteristics of GC cases in which miR-148a is downregulated. To confirm the localization of miR-148a expression, *in situ* hybridization (ISH) was carried out using GC tissues. We could detect the miR-148a expression only in fundic glands and pyloric glands. However, neither cancer cells nor stromal tissues expressed miR-148a (Fig. 1a). Then, to further understand the relationship between miR-148a expression and clinicopathologic parameters, we examined the miR-148a expression levels in 61 formalin-fixed paraffin-embedded samples of primary GC and their corresponding non-neoplastic gastric mucosa by qRT-PCR. In this sample set, miR-148a expression levels were also significantly downregulated in GC tissue compared with corresponding non-neoplastic mucosa (Fig. S2). The expression level of miR-148a was evaluated using the tumor : normal ratio of miR-148a. The relationship

Table 1. Summary of significantly downregulated miRNAs in gastric cancer tissue compared with non-neoplastic mucosa

miRBase ID	Mature accession	Intensity		Fold change	*P*-value
		Non-neoplastic mucosa	Tumor		
hsa-miR-148a	MIMAT0000243	892	279	−0.31	0.0178
hsa-miR-29a	MIMAT0000086	1626	932	−0.57	0.0395
hsa-miR-30a-3p	MIMAT0000088	681	412	−0.60	0.0246
hsa-miR-302b	MIMAT0000715	953	581	−0.61	0.0207
hsa-miR-30a-5p	MIMAT0000087	648	402	−0.62	0.0443
hsa-miR-125b-1	MIMAT0000423	1257	804	−0.64	0.0315

miRBase ID codes are available from www.mirbase.org.

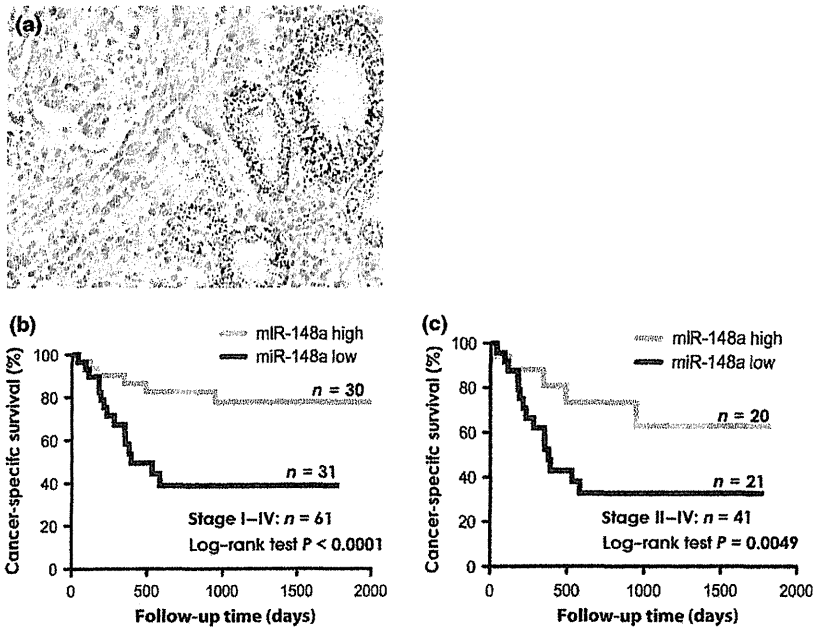

Fig. 1. *In situ* hybridization for microRNA-148a (miR-148a) and relationship between miR-148a expression and gastric caner (GC) patient prognosis. (a) MiR-148a expression in GC tissue detected by *in situ* hybridization. (b) Log–rank test and Kaplan–Meier plots were constructed for the miR-148a high and miR-148a low groups. Cancer-specific survival of 61 patients with GC based on the expression levels of miR-148a (cut-off line = median miR-148a expression level). (c) Cancer-specific survival of 41 patients with advanced (stage II–IV) GC based on the expression levels of miR-148a (cut-off line = median miR-148a expression level in this group).

Table 2. Univariate and multivariate analysis of factors influencing survival in 61 patients with gastric cancer

Parameter	Univariate analysis			Multivariate analysis		
	HR	95% CI	*P*-value	HR	95% CI	*P*-value
Sex						
Female	Ref.					
Male	1.271	0.702–1.532	0.5896	NA	NA	NA
Age, years						
<60	Ref.					
≥60	1.122	0.442–1.483	0.8593	NA	NA	NA
Mucin phenotype						
I and N type	Ref.					
G and GI type	0.903	0.214–3.802	0.1003	NA	NA	NA
Histology†						
Intestinal	Ref.					
Diffuse	1.601	0.254–1.473	0.2805	NA	NA	NA
T grade‡						
T1/2	Ref.			Ref.		
T3/4	4.886	1.136–3.225	0.0030	13.22	3.371–50.747	<0.0010
N grade‡						
N0	Ref.			Ref.		
N1/2/3	9.234	1.388–16.667	<0.0010	5.063	0.931–94.529	0.0625
Stage‡						
0/I/II	Ref.			Ref.		
III/IV	8.460	2.083–11.111	<0.0010	34.579	6.293–222.270	<0.0010
miR-148a expression						
High	Ref.			Ref.		
Low	10.820	1.785–20.000	0.0041	3.076	1.216–8.776	0.0169

†Histology was determined according to the Japanese Classification of Gastric Cancer (14th edition). ‡Tumor stage was classified according to the criteria of the International Union Against Cancer TNM classification of malignant tumors. CI, confidence interval; HR, hazard ratio; NA, not applicable; Ref., reference.

between the miR-148a expression level and clinicopathologic parameters of GC is summarized in Table S1. We also evaluated the association between miR-148a expression levels and cancer-specific mortality. In all cases and in 41 advanced GC patients, the GC tissues with lower expression levels of miR-148a showed significantly worse prognosis than those with high expression (Fig. 1b,c). In order to further evaluate the association of miR-148a expression with cancer-specific mortality, we used both univariate and multivariate Cox proportional hazards analyses (Table 2). According to the univariate analysis, T grade, N grade, stage, and miR-148a expression were significantly associated with cancer-specific mortality. According to the multivariate model, expression of miR-148a was an independent prognostic classifier of cancer-specific

mortality. These results indicate that loss of miR-148a may play important roles in GC progression.

Analysis of *MIR148A* methylation in GC cell lines. To pursue the cause of miR-148a downregulation, we examined the methylation status in CpG islands of the *MIR148a* promoter region in GC cell lines. Expression levels of miR-148a measured by qRT-PCR are shown in Figure S3(a), and we carried out bisulfite sequencing of genomic DNAs from two GC cell lines with high miR-148a expression and two cell lines with low miR-148a expression. Results of bisulfite sequencing are shown in Figure S3(b). An inverse correlation was observed between frequency of methylation in *MIR148a* promoter-region CpG islands and expression levels of miR-148a. In addition, we ascertained that miR-148a expression was restored in five aza-dc-treated MKN-45 and MKN-74 cells (Fig. S3c). These results suggest that DNA methylation of CpG islands of *MIR148A* play an important role in transcriptional inactivation in GC cell lines.

Effect of deregulation of miR-148a expression on cell growth and invasive activity. To investigate the biological significance of miR-148a in GC, we carried out an MTT assay 4 days after altering miR-148a expression. In this experiment, we used MKN-1 cells transfected with miR-148a precursor and HSC-57 cells transfected with miR-148a inhibitor. MKN-1 and HSC-57 were selected as they possessed the lowest and highest endogenous miR-148a expression among nine GC cell lines, respectively. Successful overexpression and suppression of miR-148a in each treated cell line were confirmed by qRT-PCR (Fig. 2a). Cell growth of GC cells with deregulated miR-148a expression did not differ from that of cells transfected with control miRNA up to day 4 (data not shown). Next, a Transwell invasion assay was carried out. The invasiveness of miR-148a-overexpressing MKN-1 cells was reduced compared with the negative control miRNA-transfected MKN-1 cells (Fig. 2b). In contrast, the invasiveness of miR-148a-suppressed HSC-57 cells was greater than that of the negative control miRNA-transfected HSC-57 cells (Fig. 2c). These results are consistent with those of a previous report,[22] and indicate that miR-148a regulates some genes which in turn affect tumor invasion in GC cells.

MicroRNA-148a target prediction using custom oligonucleotide array. Although some reports have identified the target gene of miR-148a, these studies used online databases to derive predicted targets.[22–25] To identify novel GC invasion-related genes whose expression was directly regulated by miR-148a, we analyzed gene expression profiles from four GC cell lines showing deregulation of miR-148a alongside corresponding non-treated cells, using a custom oligonucleotide array. In each cell line, either overexpression or suppression of miR-148a was induced, according to their endogenous miR-148a expression level. The list of genes with expression altered more than twofold in miR-148a-deregulated cells is summarized in Table 3. Among these candidates, *MMP7* was markedly downregulated by miR-148a overexpression both in MKN-45 and MKN-74 cell lines. Although target prediction for miR-148a was carried out using online databases including TargetScan, PicTar, and miRanda, these databases did not list *MMP7* as a candidate miR148a target gene (data not shown). Therefore, further study of the correlation between miR-148a and *MMP7* was undertaken.

To confirm the regulation of MMP7 by miR-148a, MKN-45 and MKN-74 cells were transfected to induce miR-148a overexpression, then examined for MMP7 expression level by Western blotting. In both cell lines, MMP7 expression was significantly downregulated; levels were similar to that of MMP7-specific siRNA treated cells (Fig. 3a). The *MMP7* mRNA levels determined by qRT-PCR were consistent with the MMP7 protein levels determined by Western blotting (Fig. 3b). It was also

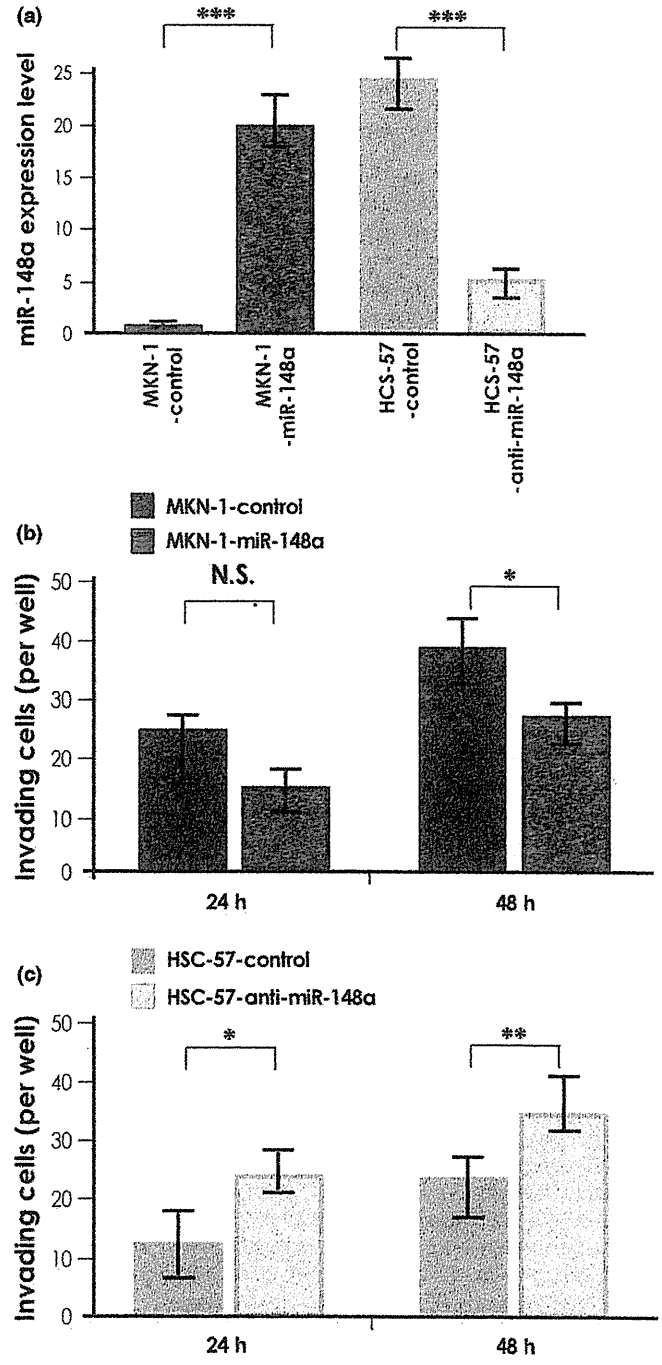

Fig. 2. MicroRNA-148a (miR-148a) expression and functional analysis. (a) Quantitative RT-PCR analysis of miR-148a in MKN-1 gastric cancer cells transfected with pre-miR-148a and HSC-57 cells transfected with anti-miR-148a. (b) Effect of miR-148a downregulation on cell invasion of MKN-1 cells. MKN-1 transfected with negative control miRNA and pre-miR-148a were incubated in Boyden chambers. (c) Effect of miR-148a downregulation on cell invasion of HSC-57 cells. HSC-57 transfected with negative control miRNA and anti-miR-148a were incubated in Boyden chambers. Results are mean ± SD of triplicate measurements. $*P < 0.05$; $**P < 0.01$; $***P < 0.001$. N.S., not significant.

Table 3. Genes downregulated by microRNA-148a (miR-148a) deregulation

Symbol	Description	GenBank	Intensity		Fold change
			Control	miR-148a	
MKN-1					
KRTHB1	Keratin 86	NM_000584.2	168	72	−2.33
CDH17	Cadherin 17, LI-cadherin	NM_001912	148	72	−2.09
APOE	Apolipoprotein E	NM_145804.1	118	57	−2.03
MKN45					
MMP7	Matrix metallopeptidase 7	NM_002423.3	730	132	−5.55
MIA	Melanoma inhibitory activity	NM_006533.3	649	244	−2.63
MKN-74					
MMP7	Matrix metallopeptidase 7	NM_002423.3	291	32	−9.99
NEIL	Nei endonuclease VIII- like 1	NM_024608.3	2004	831	−2.43
MMP1	Matrix metallopeptidase 1	NM_002421.3	455	208	−2.17
HSC-57					
MMP10	Matrix metallopeptidase 10	NM_002425.2	766	381	−2.00

found that upregulation of *MMP7* was inversely associated with miR-148a expression in GC cases analyzed in Figure 1(b) (Table S2). In addition, we examined the effect of miR-148a deregulation on the expression of epithelial–mesenchymal transition-related molecules. However, no significant alterations of these molecules were detected in miR-148a deregulated cells (Fig. S4a). As shown in Figure 2(b), overexpression of miR-148a repressed invasion of MKN-1 cells. However, MMP7 expression was not detected in MKN-1 cells (data not shown). It was reported that ROCK1 is a direct target of miR-148a and could be involved in GC invasion.[22] We checked expression of ROCK1 in MKN-1 and the alteration of its expression in miR-148a-deregulated cells. Actually, we detected that expression of ROCK1 was downregulated by miR-148a overexpression in MKN-1 cells (Fig. S4b). Furthermore, to prove that *MMP7* is a direct target of miR-148a, we used a 3′-UTR sequence of *MMP7* cloned into a reporter vector downstream of the luciferase complementary DNA (Fig. 3c). Transfection of this construct into three GC cell lines with high endogenous miR-148a expression levels led to suppression of *MMP7* reporter activity, and mutation of the miR-148a binding site abolished the inhibitory effect of miR-148a on reporter activity (Fig. 3d). Conversely, transfection of this construct into three GC cell lines with low endogenous miR-148a expression levels did not lead to suppression of *MMP7* reporter activity. However, cotransfection of this construct with miR-148a precursor into these cells showed that miR-148a suppressed the *MMP7* reporter activity (Fig. S5). These results imply that miR-148a downregulates *MMP7* expression by directly targeting its 3′-UTR.

Several reports show that miR-148a regulates cancer cell invasion through suppressing its target genes.[22,23] To confirm the cellular level at which MMP7 contributes to GC cell invasion, the MKN-45 cell line was stably transfected with vector expressing miR-148a alone, and cotransfected with vectors expressing miR-148a and MMP7. MKN-45 cells were selected because they express high levels of MMP7 and low levels of miR-148a. In MKN-45-miR-148a, which stably expressed miR-148a, MMP7 expression was significantly suppressed, and in MKN-45-miR-148a/-MMP7, which stably expressed miR-148a and MMP7, the expression of MMP7 was 50% less than that of empty vector-transfected MKN-45 cells (Fig. 3e). Next, the invasive properties of these cells were examined by Transwell invasion assay. As shown in Figure 3(f), the invasiveness of MKN-45-miR-148a was approximately 50% less than that of MKN-45-empty vector at all endpoints. However, the invasiveness of MKN-45-miR-148a/-MMP7 was only approximately 10–20% less than that of the MKN-45-empty vector. These observations suggest that MMP7 plays a central role in GC invasion among miR-148a target genes.

Discussion

In this study, we showed frequent downregulation of miR-148a in GC tissue that was significantly correlated with lymph node metastasis, advanced clinical stage, and poor clinical outcome. We also established that MMP7 is a direct and functional target of miR-148a. This is the first report to identify miRNA that regulates MMP7 expression. Further studies revealed that overexpression of miR-148a suppressed GC cell invasion *in vitro*, and cotransfection of miR-148a and MMP7 restored invasiveness of GC cells. It has been reported that MMP7 plays a key role in invasive properties of various cancer cells, and *MMP7* is well known as a representative cancer invasion-related gene whose expression is correlated with worse clinicopathologic characters.[26,27] Together with previous reports, our results suggest that miR-148a plays important roles in suppressing tumor progression in GC, and that the induction of MMP7 expression by downregulation of miR-148a contributes to GC progression.

MicroRNA microarray analysis and qRT-PCR revealed that miR-148a was significantly downregulated in GC tissue, and we also confirmed that hypermethylation of *MIR148A* CpG islands is correlated with suppression of miR-148a in GC cell lines. It has been reported that hypermethylation of *MIR148A* CpG islands is induced by DNA methyltransferase-1, however DNA methyltransferase-1, in turn, is conversely downregulated by miR-148a overexpression.[28] In healthy stomach tissue, next-generation sequencing reportedly confirms overexpression of miR-148a,[29] and downregulation of miR-148a has been reported in various cancers including GC.[30–32] In relation to miR-148a, almost all of its target genes were implicated in promoting cancer progression. These results suggest that miR-148a may play essential roles in maintaining homeostasis of normal stomach tissue, and when downregulated, sequential induction of some oncogenes may contribute to the development of gastric neoplasia. However, the points at which downregulation of miR-148a occurs in the process of carcinogenesis

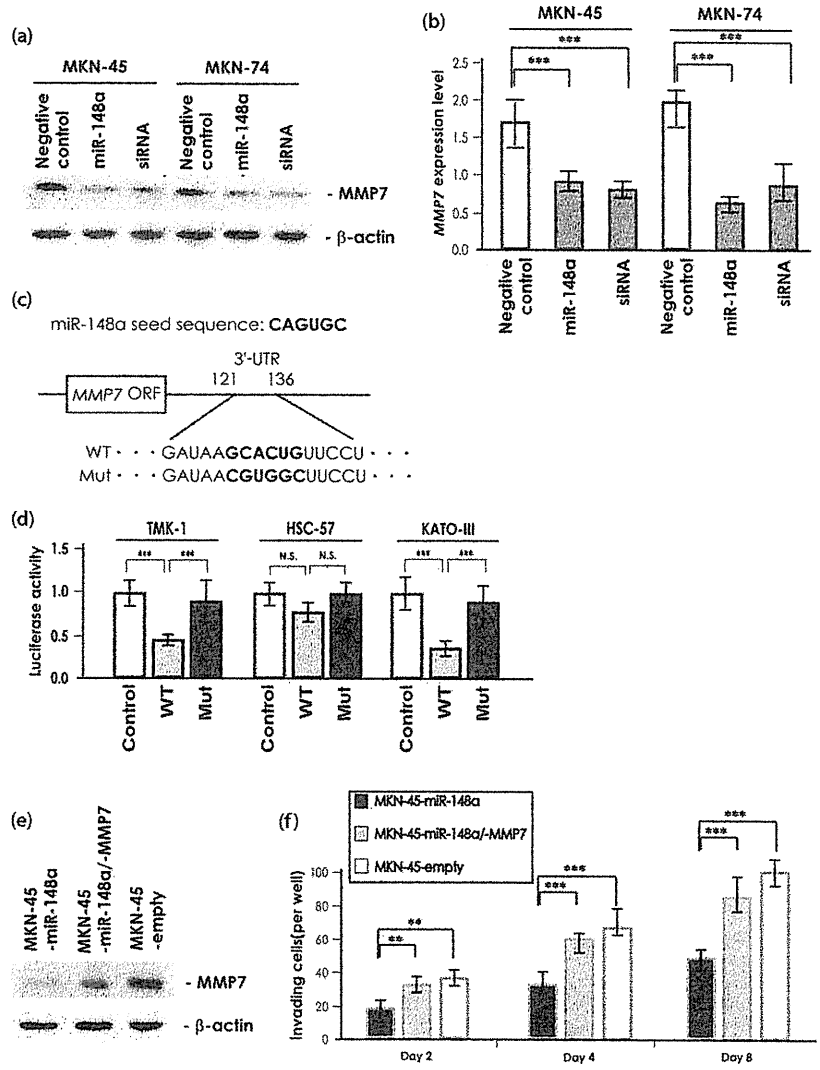

Fig. 3. Effect of microRNA-148a (miR-148a) on MMP7 expression and gastric cancer (GC) cell invasiveness. (a) Western blot analysis of MMP7 in MKN-45 and MKN-74 cell lysates after treatment with negative control miRNA, pre-miR-148a, or MMP7-specific siRNA. A β-actin blot served as loading control. (b) Quantitative RT-PCR analysis of *MMP7* in MKN-45 and MKN-74 cells after treatment with negative control miRNA, pre-miR-148a, or MMP7-specific siRNA. Results are mean ± SD of triplicate measurements. $^{***}P < 0.001$. (c) Schematic representation of miR-148a seed sequence and *MMP7* 3′-UTR, showing the putative miR-148a-binding site. The seed region is in bold text and the seed region is mutated in the reporter construct. (d) Luciferase activity of three GC cell lines cotransfected with reporter vector containing either control vector, wild-type (WT), or mutant miR-148a (Mut) 3′-UTR. Results are mean ± SD of triplicate measurements. $^{***}P < 0.001$. N.S., not significant. (e) Western blot analysis of MMP7 in MKN-45 cell lysates was carried out after stable transfection with the miR-148a construct, both miR-148a and MMP7 construct, or empty vector. β-Actin served as loading control. (f) Effect of miR-148a-stable transfection and restoration of MMP7 on cell invasion of MKN-45 cells. Boyden chambers were used for incubation of MKN-45 cells after stable transfection with miR-148a construct, both miR-148a and MMP7 construct, or empty vector. Results are mean ± SD of triplicate measurements. $^{**}P < 0.01$; $^{***}P < 0.001$.

or tumor progression have not been fully elucidated. In GC, there is no report that has examined the timing of miR-148a downregulation. It is our current important task to determine when miR-148a is downregulated in gastric neoplasia.

A number of miRNA target-prediction databases have been developed and tested for accuracy and precision using both computational and laboratory techniques. However, when results from laboratory techniques were compared to those of computational approaches, analysis showed that most gene lists generated using computational target prediction contained high false-negative and false-positive results.[7,33] In addition, various miRNA target prediction programs, which use different algorithms of targeting, produce different lists of predicted targets. It is documented that these differences can arise from the source of 3′-UTR sequences. In the present study, using custom oligonucleotide array-based target prediction, we found that MMP7 expression is downregulated by miR-148a overexpression. Moreover, this was confirmed by qRT-PCR, Western blotting, and reporter gene assays. We determined the 3′-UTR of *MMP7* by referring to the Gene database available from the National Center for Biotechnology Information (NCBI), and found that the 3′-UTR of *MMP7* contains a putative binding site that is complementary to the miR-148a seed sequence. We compared the sequence of *MMP7* coding region from the Gene database (NCBI: http://www.ncbi.nlm.nih.gov) with that from Ensembl (http://useast.ensembl.org) or UCSC (http://genome.ucsc.edu). Although slight differences were observed among these sequences, including the definition of the start point, most were almost completely matched. This result suggests that the extant online miRNA target prediction database did not detect *MMP7* as a candidate target gene of miR-148a, due to a deficiency in their chosen algorithm. These considerations point to a need for further refinement of online databases, in order to effectively identify real target genes for any given miRNA. At this point in time, conventional laboratory techniques remain very valuable methods for effective identification of miRNA target genes.

In summary, we have shown that downregulation of miR-148a is an independent prognostic classifier in patients with GC. Furthermore, this study identified MMP7 as a direct target of miR-148a in GC cells and its restoration by downregulation of miR-148a in these cells increases tumor invasive activity. The present findings provide evidence for the contribution of miR-148a to the maintenance of homeostasis in normal stomach tissue and suggest an additional role for miR-148a in GC invasion through regulation of MMP7 expression. Elucidation

of a fuller picture of the molecular mechanisms through which miR-148a is involved in gene deregulatory oncogenic processes could improve our understanding of carcinogenesis, particularly tumor progression in GC.

Acknowledgments

We thank Mr. Shinichi Norimura for excellent technical assistance. This work was carried out with the kind cooperation of the Research Center for Molecular Medicine, Faculty of Medicine, Hiroshima University (Hiroshima, Japan). We thank the Analysis Center of Life Science, Hiroshima University, for the use of their facilities. This work was supported by Grants-in-Aid for Research from the Ministry of Education, Culture, Science, Sports, and Technology of Japan, and, in part, by a Grant-in-Aid for the Third Comprehensive 10-Year Strategy for Cancer Control and for Cancer Research from the Ministry of Health, Labor, and Welfare of Japan, and from The National Institute of Biomedical Innovation (Program for Promotion of Fundamental Studies in Health Sciences). This work was also supported in part by a Research Fellowship of the Japan Society for the Promotion of Science and the National Cancer Center Research and Development Fund (23-A-9).

Disclosure Statement

The authors have no conflict of interest.

References

1 Crew KD, Neugut AI. Epidemiology of gastric cancer. *World J Gastroenterol* 2006; **12**: 354–62.
2 Yasui W, Sentani K, Sakamoto N, Anami K, Naito Y, Oue N. Molecular pathology of gastric cancer: research and practice. *Pathol Res Pract* 2011; **207**: 608–12.
3 Calin GA, Croce CM. MicroRNA signatures in human cancers. *Nat Rev Cancer* 2006; **6**: 857–66.
4 Bartel DP. MicroRNAs: genomics, biogenesis, mechanism, and function. *Cell* 2004; **116**: 281–97.
5 Ambros V. The functions of animal microRNAs. *Nature* 2004; **431**: 350–5.
6 Di Leva G, Croce CM. Roles of small RNAs in tumor formation. *Trends Mol Med* 2010; **16**: 257–67.
7 Alexiou P, Maragkakis M, Papadopoulos GL, Reczko M, Hatzigeorgiou AG. Lost in translation: an assessment and perspective for computational microRNA target identification. *Bioinformatics* 2009; **25**: 3049–55.
8 Thomson DW, Bracken CP, Goodall GJ. Experimental strategies for microRNA target identification. *Nucleic Acids Res* 2011; **39**: 6845–53.
9 Zhao X, Dou W, He L *et al.* MicroRNA-7 functions as an anti-metastatic microRNA in gastric cancer by targeting insulin-like growth factor-1 receptor. *Oncogene* 2013; **32**: 1363–72.
10 Tsukamoto Y, Nakada C, Noguchi T *et al.* MicroRNA-375 is downregulated in gastric carcinomas and regulates cell survival by targeting PDK1 and 14-3-3zeta. *Cancer Res* 2010; **70**: 2339–49.
11 Sakamoto N, Oue N, Noguchi T *et al.* Serial analysis of gene expression of esophageal squamous cell carcinoma: ADAMTS16 is upregulated in esophageal squamous cell carcinoma. *Cancer Sci* 2010; **101**: 1038–44.
12 Nagao K, Togawa N, Fujii K *et al.* Detecting tissue-specific alternative splicing and disease-associated aberrant splicing of the PTCH gene with exon junction microarrays. *Hum Mol Genet* 2005; **14**: 3379–88.
13 Oue N, Sentani K, Sakamoto N *et al.* Characteristic gene expression in stromal cells of gastric cancers among atomic-bomb survivors. *Int J Cancer Suppl* 2009; **124**: 1112–21.
14 Kondo T, Oue N, Yoshida K *et al.* Expression of POT1 is associated with tumor stage and telomere length in gastric carcinoma. *Cancer Res* 2004; **64**: 523–9.
15 Shinmei S, Sakamoto N, Goto K *et al.* MicroRNA-155 is a predictive marker for survival in patients with clear cell renal cell carcinoma. *Int J Urol* 2013; **20**: 468–77.
16 Yasui W, Sano T, Nishimura K *et al.* Expression of P-cadherin in gastric carcinomas and its reduction in tumor progression. *Int J Cancer Suppl* 1993; **54**: 49–52.
17 Herman JG, Graff JR, Myohanen S, Nelkin BD, Baylin SB. Methylation-specific PCR: a novel PCR assay for methylation status of CpG islands. *Proc Natl Acad Sci USA* 1996; **93**: 9821–6.
18 Hanoun N, Delpu Y, Suriawinata AA *et al.* The silencing of microRNA 148a production by DNA hypermethylation is an early event in pancreatic carcinogenesis. *Clin Chem* 2010; **56**: 1107–18.
19 Matsumura S, Oue N, Mitani Y, Kitadai Y, Yasui W. DNA demethylation of vascular endothelial growth factor-C is associated with gene expression and its possible involvement of lymphangiogenesis in gastric cancer. *Int J Cancer Suppl* 2007; **120**: 1689–95.
20 Sakamoto N, Oue N, Sentani K *et al.* Liver-intestine cadherin induction by epidermal growth factor receptor is associated with intestinal differentiation of gastric cancer. *Cancer Sci* 2012; **103**: 1744–50.
21 Alley MC, Scudiero DA, Monks A *et al.* Feasibility of drug screening with panels of human tumor cell lines using a microculture tetrazolium assay. *Cancer Res* 1988; **48**: 589–601.
22 Zheng B, Liang L, Wang C *et al.* MicroRNA-148a suppresses tumor cell invasion and metastasis by downregulating ROCK1 in gastric cancer. *Clin Cancer Res* 2011; **17**: 7574–83.
23 Aprelikova O, Palla J, Hibler B *et al.* Silencing of miR-148a in cancer-associated fibroblasts results in WNT10B-mediated stimulation of tumor cell motility. *Oncogene* 2013; **32**: 3246–53.
24 Cheng P, Chen C, He HB *et al.* MiR-148a regulates osteoclastogenesis via targeting MAFB. *J Bone Miner Res* 2013; **28**: 1180–90.
25 Song H, Wang Q, Wen J *et al.* ACVR1, a therapeutic target of fibrodysplasia ossificans progressiva, is negatively regulated by miR-148a. *Int J Mol Sci* 2012; **13**: 2063–77.
26 Fanelli MF, Chinen LT, Begnami MD *et al.* The influence of transforming growth factor-alpha, cyclooxygenase-2, matrix metalloproteinase (MMP)-7, MMP-9 and CXCR4 proteins involved in epithelial-mesenchymal transition on overall survival of patients with gastric cancer. *Histopathology* 2012; **61**: 153–61.
27 Iguchi H, Kosaka N, Ochiya T. Versatile applications of microRNA in anticancer drug discovery: from therapeutics to biomarkers. *Curr Drug Discov Technol* 2010; **7**: 95–105.
28 Zhu A, Xia J, Zuo J *et al.* MicroRNA-148a is silenced by hypermethylation and interacts with DNA methyltransferase 1 in gastric cancer. *Med Oncol* 2012; **29**: 2701–9.
29 Ribeiro-dos-Santos A, Khayat AS, Silva A *et al.* Ultra-deep sequencing reveals the microRNA expression pattern of the human stomach. *PLoS One* 2010; **5**: e13205.
30 Ueda T, Volinia S, Okumura H *et al.* Relation between microRNA expression and progression and prognosis of gastric cancer: a microRNA expression analysis. *Lancet Oncol* 2010; **11**: 136–46.
31 Chen Y, Song Y, Wang Z *et al.* Altered expression of MiR-148a and MiR-152 in gastrointestinal cancers and its clinical significance. *J Gastrointest Surg* 2010; **14**: 1170–9.
32 Liffers ST, Munding JB, Vogt M *et al.* MicroRNA-148a is down-regulated in human pancreatic ductal adenocarcinomas and regulates cell survival by targeting CDC25B. *Lab Invest* 2011; **91**: 1472–9.
33 Bentwich I. Prediction and validation of microRNAs and their targets. *FEBS Lett* 2005; **579**: 5904–10.

Supporting Information

Additional supporting information may be found in the online version of this article:

Fig. S1. Comparison between microarray and quantitative RT-PCR data for microRNA-148a (miR-148a) expression levels in the same gastric cancer (GC) sample set.

Fig. S2. Comparison between microRNA-148a (miR-148a) expression levels in non-neoplastic gastric mucosa and gastric cancer (GC).

Fig. S3. Quantitative RT-PCR and bisulfite genomic DNA sequencing analysis of *MIR148A* in gastric cancer (GC) cell lines.

Fig. S4. Effect of microRNA-148a (miR-148a) on epithelial–mesenchymal transition-related molecules and ROCK1 expression in gastric cancer cell lines.

Fig. S5. Effect of microRNA-148a (miR-148a) on MMP7 expression in gastric cancer cell lines.

Table S1. Correlation between microRNA-148a (miR-148a) expression level and clinicopathologic characters.

Table S2. Correlation between *MMP7* and microRNA-148a (miR-148a) expression in gastric cancer tissue.

Data S1. Materials and methods.

OPEN ACCESS

ORIGINAL ARTICLE

Canonical Wnt signals combined with suppressed TGFβ/BMP pathways promote renewal of the native human colonic epithelium

Amy Reynolds,[1] Natalia Wharton,[1] Alyson Parris,[1] Esther Mitchell,[1] Anastasia Sobolewski,[2] Christy Kam,[1] Loren Bigwood,[1] Ahmed El Hadi,[1] Andrea Münsterberg,[1] Michael Lewis,[3] Christopher Speakman,[3] William Stebbings,[3] Richard Wharton,[3] Kevin Sargen,[3] Richard Tighe,[4] Crawford Jamieson,[4] James Hernon,[3] Sandeep Kapur,[3] Naohide Oue,[5] Wataru Yasui,[5] Mark R Williams[1]

▶ Additional material is published online only. To view please visit the journal online (http://dx.doi.org/10.1136/gutjnl-2012-304067).

[1]School of Biological Sciences, University of East Anglia, Norwich Research Park, Norwich, Norfolk, UK
[2]Department of Gut Health and Food Safety, Institute Strategic Programme, Institute of Food Research, Colney, Norwich Research Park, Norwich, Norfolk, UK
[3]Department of Surgery, Norfolk and Norwich University Hospitals Trust, Colney Lane, Norwich Research Park, Norwich, Norfolk, UK
[4]Department of Gastroenterology, Norfolk and Norwich University Hospitals Trust, Colney Lane, Norwich Research Park, Norwich, Norfolk, UK
[5]Department of Molecular Pathology, Hiroshima University Institute of Biomedical and Health Sciences, Hiroshima, Japan

Correspondence to
Dr Mark R Williams, School of Biological Sciences, University of East Anglia, Norwich Research Park, Norwich, Norfolk NR47TJ, UK;
m.r.williams@uea.ac.uk

AR, NW and AP contributed equally.

Received 5 November 2012
Revised 29 May 2013
Accepted 31 May 2013
Published Online First
5 July 2013

To cite: Reynolds A, Wharton N, Parris A, *et al*. *Gut* 2014;**63**:610–621.

ABSTRACT

Background A defining characteristic of the human intestinal epithelium is that it is the most rapidly renewing tissue in the body. However, the processes underlying tissue renewal and the mechanisms that govern their coordination have proved difficult to study in the human gut.

Objective To investigate the regulation of stem cell-driven tissue renewal by canonical Wnt and TGFβ/bone morphogenetic protein (BMP) pathways in the native human colonic epithelium.

Design Intact human colonic crypts were isolated from mucosal tissue samples and placed into 3D culture conditions optimised for steady-state tissue renewal. High affinity mRNA in situ hybridisation and immunohistochemistry were complemented by functional genomic and bioimaging techniques. The effects of signalling pathway modulators on the status of intestinal stem cell biology, crypt cell proliferation, migration, differentiation and shedding were determined.

Results Native human colonic crypts exhibited distinct activation profiles for canonical Wnt, TGFβ and BMP pathways. A population of intestinal LGR5/OLFM4-positive stem/progenitor cells were interspersed between goblet-like cells within the crypt-base. Exogenous and crypt cell-autonomous canonical Wnt signals supported homeostatic intestinal stem/progenitor cell proliferation and were antagonised by TGFβ or BMP pathway activation. Reduced Wnt stimulation impeded crypt cell proliferation, but crypt cell migration and shedding from the crypt surface were unaffected and resulted in diminished crypts.

Conclusions Steady-state tissue renewal in the native human colonic epithelium is dependent on canonical Wnt signals combined with suppressed TGFβ/BMP pathways. Stem/progenitor cell proliferation is uncoupled from crypt cell migration and shedding, and is required to constantly replenish the crypt cell population.

Significance of this study

What is already known about this subject?

- In the mouse, renewal of the intestinal epithelium is regulated by signalling cross-talk between the Wnt, Notch, epidermal growth factor (EGF) and TGFβ/BMP pathways.
- Wnt signals predominate at the intestinal crypt-base and maintain intestinal stem cell biology.
- LGR5, a Wnt target gene, is a marker for mouse intestinal stem cells.
- Wnt signals are required for the development of mouse intestinal organoids from single intestinal stem cells in culture.
- Additional pharmacological strategies have led to the development of spheroid and budding organoid systems for the long-term culture of human intestinal stem cells.

What are the new findings?

- Tissue renewal in the native human colonic epithelium can be studied in real time ex vivo.
- Wnt signals in combination with suppressed TGFβ/BMP pathways maintain the hierarchy and procession of tissue renewal along the human colonic crypt-axis.
- A population of proliferative LGR5/OLFM4-positive stem/progenitor cells are supported by Wnt signals at the crypt-base.
- We propose that crypt cell migration and shedding is the default state and that Wnt signals are required for steady-state tissue renewal.

How might it impact on clinical practice in the foreseeable future?

- The native human colonic crypt culture model will permit functional interrogation of the status and mechanisms underlying tissue renewal in the healthy ageing human colonic epithelium and in tissue at risk of disease.
- The use of native human tissue will help the development and translation of novel strategies for the prevention of cancer and inflammatory bowel disease.

INTRODUCTION

Along with other self-renewing tissues such as skin and bone marrow, the mammalian gut epithelium is one of the most dynamic tissues in the body. The constant renewal cycle is of 5–7 days duration and takes place in a hostile environment characterised by the presence of bacterial toxins and metabolites,

dietary antigens and mutagens, and immunological cytokines and oxidative stress. Approximately 10 billion cells are shed from the gut epithelium each day and these are continuously replaced by intestinal stem cell progeny. The colonic epithelium is exquisitely organised into millions of invaginations called crypts, each of which represents the self-renewing unit of the tissue. At the base of every crypt, it is thought that intestinal stem cells divide symmetrically to self-renew and undertake a progenitor phenotype on exiting the stem cell niche.[1 2] Stem cell progeny (transit amplifying cells) proliferate, migrate and differentiate (into enterocytes, goblet cells, enteroendocrine cells and tuft cells) along the crypt-axis before they are shed from the surface epithelium. The hierarchy of tissue renewal is thought to minimise the accumulation of molecular damage by virtue of positioning long-lived stem cells in a relatively safe harbour at the crypt-base, from where they fuel the constant replenishment of shed cells. The molecular mechanisms that regulate the physiological processes of tissue renewal are of the utmost interest because they are disrupted in conditions such as inflammatory bowel disease and colon cancer.

A small number of highly conserved signalling pathways that play a key role in developmental biology have also been implicated in regulating the hierarchy of intestinal tissue renewal in the adult. A series of elegant studies in the mouse have suggested that reciprocal morphogenic gradients along the crypt-axis orchestrate stem/progenitor cell proliferation, lineage specification, migration, differentiation and shedding.[3 4] The canonical Wnt signalling pathway has been deemed the master regulator of intestinal tissue renewal.[5] Adenoviral and transgenic expression of DKK-1, an inhibitor of the canonical Wnt signalling pathway, decimated the presence of mouse intestinal crypts.[6 7] Coupled to the predominance of canonical Wnt signals at the intestinal crypt-base, this led to the discovery that the Wnt target gene *lgr5* was enriched in mouse intestinal stem cells[8] and that ligation of this membrane receptor by the intestinotrophic factor R-spondin-1,[9] in conjunction with Wnt ligand-Fz-LRP5/6 complex formation,[10 11] synergistically activated Wnt signals. These seminal studies have given rise to the consensus that intense canonical Wnt signals at the crypt-base support intestinal stem cell biology (and Paneth cell differentiation in the small intestine) and that diminished Wnt signalling intensity along the crypt-axis is an important cue for progenitor proliferation, lineage specification, migration and shedding. Conversely, TGFβ/BMP signals predominate towards the open end of the crypt where they are thought to influence crypt cell positioning, differentiation and apoptosis.[12–15]

An analysis of gene expression patterns of normal human 'colon tops and basal crypts'[16] has detailed the topological expression of signalling pathway activators and inhibitors that are predicted to establish morphogenic gradients along the human colonic crypt-axis. Intriguingly, the respective activity of the Wnt signalling pathway at the crypt-base and the TGFβ/BMP pathway at the crypt-top is not thought not to be mutually exclusive. Reciprocal inhibition of the Wnt and TGFβ/BMP pathways appears to maintain the hierarchy and procession of tissue renewal along the crypt-axis. For example, genetic approaches in the mouse and analysis of human polyposis syndromes and colon cancer suggest that loss of TGFβ/ BMP pathway activation augments the Wnt signalling pathway, which disrupts tissue renewal and drives intestinal polyp/tumour formation.[12 14 15 17–19] In keeping with this notion, tissue culture conditions that favour Wnt pathway activation and inhibition of the TGFβ/BMP pathways have permitted the expansion ad infinitum of mouse and human intestinal organoids ex vivo. Strikingly, single crypts derived from the human colon spawn multiple budding structures[20] or expand into cyst-like spheroids,[21] each composed predominantly of immature stem/progenitor cells that can be induced to differentiate by withdrawal of Wnt stimulation, or used for therapeutic transplantation.[22] However, a detailed knowledge of the processes and signalling pathways involved in stem cell-driven tissue renewal in the human colonic epithelium is still lacking and is required to understand more fully the risk and pathogenesis of colorectal disease.

We have developed a culture model of near-native human colonic crypts that preserves crypt length, topology, morphology and cellular polarity.[23] Significantly, we now demonstrate that the hierarchy of stem cell-driven tissue renewal is recapitulated within this near-native human colonic crypt model ex vivo. Real-time imaging, gene reporter assays and dominant negative gene expression, in combination with subcellular immunolocalisation and in situ hybridisation, have been used to assess the status and mutual influence of Wnt and TGFβ/BMP signals on intestinal stem cell biology, proliferation, differentiation, migration and cell shedding in near-native human colonic crypts.

MATERIAL AND METHODS

Human colorectal tissue samples

This study was performed in accordance with approval from the East of England National Research Ethics Committee (LREC 97/124). Colorectal tissue samples were obtained with informed consent at rectosigmoid endoscopy from the sigmoid colon of 52 patients (51–83 years old) exhibiting no apparent intestinal pathology and from the normal mucosa (ie, >10 cm tumour margin) of 30 patients undergoing anterior resection (44–85 years old).

Microdissection of fixed native human colonic crypts

Biopsy tissue samples or surgical mucosal specimens were immediately fixed with 4% paraformaldehyde for 1 h and placed in phosphate-buffered saline. Single microdissected crypts were embedded in Matrigel, postfixed with 4% paraformaldehyde and processed for immunohistochemistry (see online supplementary methods).

Human colonic crypt isolation and culture

Colonic crypts were isolated as described previously,[23 24] embedded in Matrigel and placed into culture conditions that were similar to those described recently for intestinal organoids[20] and spheroids.[20 21] See online supplementary methods for details. BrdU (10 μM) was added to the experimental crypt culture media as described to monitor crypt cell proliferation and migration.

Adenoviral and lentiviral transduction

When required, freshly isolated colonic crypts were transduced with the lentiviral TOP-green fluorescence protein (GFP) Wnt reporter (HIV-based, VSV-G; SABiosciences) or adenoviral CMV-DN-TCF4 (type 5, dE1E3; Vector Biolabs) at a multiplicity of infection of 250 TU/crypt cell. Transduction with lentiviral or adenoviral CMV-GFP was used as a positive control to monitor infection efficiency.

Time-lapse videomicroscopy

Colonic crypts cultured in 12 well plates were placed on the climate-controlled (37°C, 5% CO_2) stage of a Nikon or Zeiss inverted motorised time-lapse system.

Whole mount immunohistochemistry and mRNA in situ hybridisation

Following embedding in Matrigel, microdissected-native crypts or cultured crypts were processed for immunohistochemistry or dual mRNA in situ hybridisation/immunohistochemistry. Immmunolabelling was visualised by using an appropriate combination of species-specific Alexafluor-conjugated secondary antibodies (Invitrogen). See online supplementary methods for details.

Reverse transcriptase polymerase chain reaction

Expression of marker genes for stem cells, differentiated crypt cell types and signalling pathway components was determined in freshly isolated and cultured crypts using quantitative or standard reverse transcriptase polymerase chain reaction (RT-PCR) techniques. See online supplementary methods for details.

Confocal microscopy

Following in situ hybridisation and/or immunohistochemistry, whole-mounted microdissected (ie, native) and cultured crypts were visualised by laser scanning confocal microscopy (Zeiss 510 META). A ×63 (1.4 numerical aperture) objective was used to obtain confocal images of the longitudinal crypt-axis. Image stacks were taken at 1–3 μm intervals which allowed selection of precise focal planes. The same acquisition parameters were used prior to post-hoc comparison of immunolabelling fluorescence intensity.

Image analysis

The crypt hierarchy was divided into three regions along the crypt-axis, each containing an equal number of nuclei and designated base, mid and top. In some cases, the base was subdivided into two regions of equivalent cell number, termed base and supra-base. The percentage number of cells (or nuclei) positive for a specific marker (eg, Ki67, LGR5), or the relative immunofluorescence intensity (eg, nuclear axin 2), was quantified (ImageJ, NIH) and expressed for each region; these values were either absolute or relative to the corresponding crypt-base value. Three dimensional images were rendered in Volocity (Improvision).

Statistical analysis

Data are expressed as means±SEM (n is the number of crypts derived from N patients). Differences between groups were determined using one-way analysis of variance (ANOVA) and Tukey's post-hoc method of multiple comparisons. Correlation between two variables was determined by the Spearman Rank test and independent association between variables was determined by the Chi Squared test. The level of significance (p value) is indicated in all cases.

RESULTS

Wnt, TGFβ and BMP signals correlate with the hierarchy of stem cell-driven tissue renewal in the human colonic epithelium

The hierarchy of tissue renewal in the native human colonic epithelium was characterised in crypts microdissected from colorectal biopsy tissue samples. Ki67 immunolabelling patterns depicted a prototypical profile of intense crypt cell proliferation in the lower half of the crypt-axis, including the presumptive stem cell zone at the crypt-base (figure 1A,B). Dual immunolocalisation and in situ hybridisation using high affinity oligonucleotide probes was used to visualise a population of slender LGR5-mRNA/OLFM4-positive cells (figure 1C,D; see online supplementary figure S1A) interspersed between MUC2-positive goblet-like cells (see online supplementary figure S1B) located at the base of native human colonic crypts. OLFM4 is a secretory protein[25] and was located at the mid-cell/juxtanuclear position and at the apical pole of the slender cytoplasm facing the crypt-lumen, where secreted OLFM4 protein was also present (figure 1C,D). *LGR5* mRNA labelling was perinuclear and some cells exhibited intense labelling in the mid-cell/juxtanuclear position (marked by arrowheads in figure 1C). Positive and negative controls for in situ hybridisation are shown in online supplementary figure S2. Immunolabelling using a monoclonal LGR5 antibody faithfully reproduced a similar pattern of labelling that was congruent with $OLFM4^+$ cells at the crypt-base (figure 1D). LGR5 protein was expressed on the basal membrane and within the cytoplasm of these slender crypt-base cells. As for *LGR5* mRNA in situ hybridisation, there was a subset of cells more intensely labelled with the LGR5 antibody (marked by arrowheads in figure 1D). Notably, the basal membranes of two $LGR5^+$ cells often wrapped around the basal membrane of an intervening goblet-like cell (see red arrowhead in figure 1D), which were negative for LGR5 and OLFM4 (see online supplementary figures S1B and S3B, respectively). Careful tracking in the z-dimension of E-cadherin-labelled single cell outlines, which often dipped in and out of any single confocal image plane, revealed a congruence of 96±4% for OLFM4 and either lgr5-mRNA or LGR5 protein expression; see online supplementary data for a schematic interpretation (see online supplementary figure S1A) and a 3D reconstruction (see online supplementary movie S1) of figure 1D. The $OLFM4^+/LGR5^+$ cell population predominates at the crypt-base (figure 1E) and at any one time, approximately half of the $OLFM4^+$ population is Ki67-positive (figure 1F), which is in keeping with the proliferative phenotype of mouse intestinal stem cells.[8]

An insight into the cellular signals that govern human intestinal tissue renewal was gained by spatially correlating signalling pathway activation along the hierarchy of the crypt-axis. Nuclear β-catenin, a hallmark of the canonical Wnt signalling pathway activation, and nuclear axin-2, a Wnt target gene, predominated at the crypt-base and exhibited an immunofluorescence intensity gradient that diminished along the crypt-axis (figure 2A,B). A high degree of congruence at the crypt-base was also exhibited by β-catenin and c-myc (another Wnt target gene) (see online supplementary figure S1D). Conversely, nuclear phospho-SMAD 2/3 immunofluorescence, an indicator of TGFβ pathway activation, peaked in the mid-crypt region (figure 2C), whereas nuclear phospho-SMAD 1/5/8 immunofluorescence, an indicator of BMP pathway activation, exhibited a retrogradient that was more intense at the crypt-opening (figure 2D). In accordance with similar observations made largely of the mouse intestine,[5–7 12 13 26] these findings suggested that active Wnt signals support human colonic crypt stem/progenitor cell proliferation and that TGFβ/BMP pathway activation may favour cell cycle withdrawal.

Combined activation of the Wnt pathway and inhibition of TGFβ/BMP pathways maintain native human colonic crypt morphology in culture

In order to investigate the functional influence of Wnt and TGFβ/BMP signalling pathways on renewal of the human colonic epithelium, we refined a native human colonic crypt culture model.[23] Following on from the signalling pathway profiles described in figure 2 and the conditions developed for intestinal organoid propagation,[20 21 27] optimisation of human colonic crypt culture conditions was based on generating Wnt

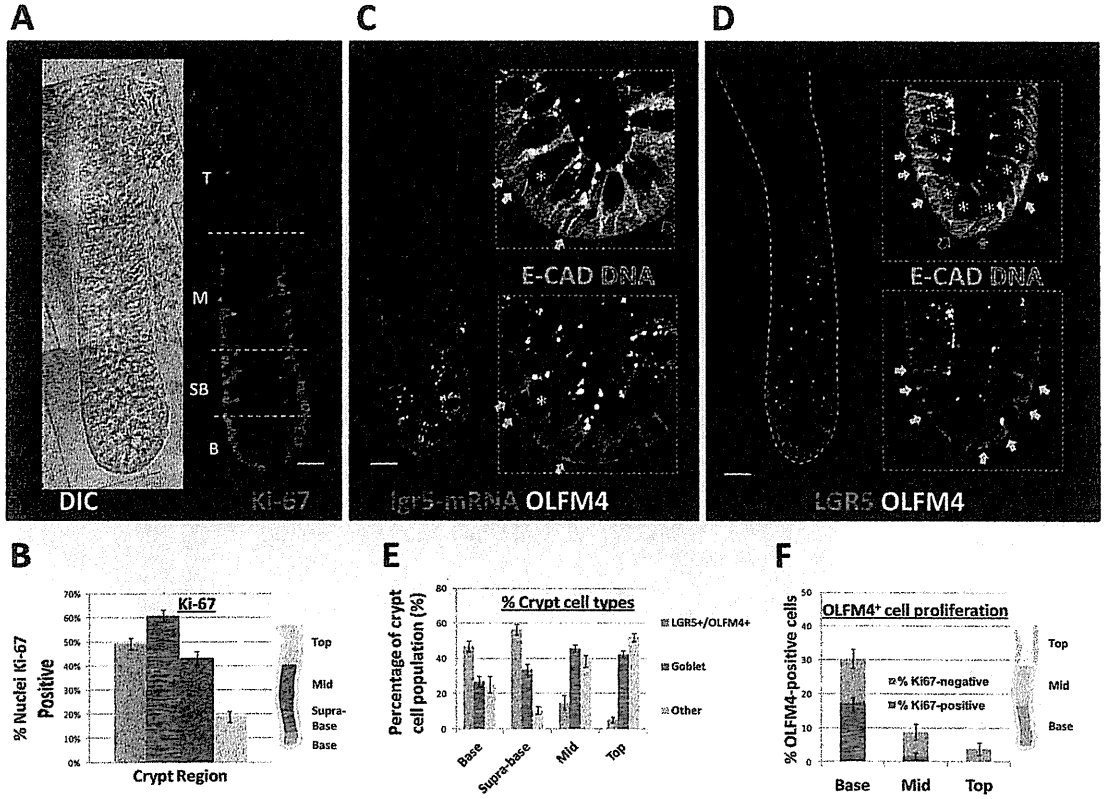

Figure 1 Hierarchy of stem/progenitor cell proliferation along the native human colonic crypt-axis. (A) Classical profile for Ki-67 immunolabelling (red) of microdissected (ie, native) human colonic crypts; B-base, SB supra-base, M-mid, T-top. (B) Ki67-positive cell nuclei predominate at the crypt-base and the mid-crypt region (N=13 subjects, n=58 crypts). (C) Dual in situ hybridisation and immunolabelling of lgr5-mRNA (red) and OLFM4 protein (white) identifies a population of lgr5-mRNA+/OLFM4+cells at the base of native human colonic crypts; E-CAD (green) demarks crypt cell membranes; filled white arrows indicate cells exhibiting intense fluorescent labelling for lgr5-mRNA and OLFM4; open arrow denotes nucleus of pericryptal myofibroblast; asterisk signifies a goblet cell with nucleus in the confocal image plane; scale bar—30 mm. (D) Double immunolabelling of LGR5 protein (red) and OLFM4 (white) confirms congruent expression of both intestinal stem cell markers by individual crypt cells within the crypt-base; annotations as above; see online supplementary figure S1 for schematic representation. (E) Quantification of cell types according to stem cell marker expression and cell morphology along the crypt-axis (see online supplementary figure S1 for an example, of lgr5-mRNA/MUC-2 double labelling); the congruence of OLFM4 and either lgr5-mRNA or LGR5 protein expression was 96%±4% (mean±SD, n=20 microdissected crypts from N=4 subjects). (F) Analysis of crypt stem/progenitor cell proliferation (n=10 crypts from N=5 subjects; see online supplementary figure S1 for a crypt image of double OLFM4/Ki-67 immunolabelling). Arrows indicate examples of intense labelling for lgr5+/OLFM4+ stem cells. *Denotes an example of a goblet cell with nucleus in plane of focus. DIC, differential interference contrast; E-CAD, E-cadherin.

signals and suppressing TGFβ/BMP signals ex vivo. A range of growth factors in various combinations were tested with the aim, in the first instance, of maintaining near-native crypt length, topology, morphology and polarity (figure 3A,B, see online supplementary figure S4). Significantly, canonical Wnt pathway activation by Wnt-3A and/or R-Spondin-1 was insufficient to maintain human colonic crypt length (figure 3D) or viability beyond 4 days (not shown). However, in combination with the BMP antagonist Gremlin-1[16] or noggin,[8] the intestinotrophic factor IGF-1,[28] and an ALK4/5/7 inhibitor A83–01 (or SB431542, not shown), crypts maintained their length and morphology for at least 7 days in culture (figure 3C,D) when the Matrigel became unstable. These conditions were conducive for crypt cell proliferation and migration as observed under digital video time-lapse microscopy (see online supplementary movies S2 and S3). Conversely, colonic crypt length and morphology were compromised by inhibition of canonical Wnt signals or by imposing either TGFβ or BMP signals (see online supplementary figure S5). Of note, replacing IGF-1 with EGF promoted remodelling of human colonic crypt morphology followed by multiple budding events characteristic of intestinal organoid growth (see online supplementary figure S6).[20]

Colonic crypt Wnt signals are inhibited by TGFβ or BMP pathway activation

To determine activation of the canonical Wnt signalling pathway, human colonic crypts were treated with Wnt-3A in the presence or absence of DKK-1. Wnt-3A stimulated translocation of nuclear de-phospho-β-catenin and this was inhibited by DKK-1 (figure 4A). Wnt-3A treatment also induced nuclear accumulation of the Wnt target gene Axin-2, which was inhibited by transduction of crypts with an adenoviral vector carrying a dominant negative TCF4 mutant (figure 4B). Exogenous Wnt-3A also stimulated TOP-GFP intensity confirming activation of Wnt target gene transcription (figure 4C). Treatment of crypts with an inhibitor of Wnt production, IWP2 (2 μM), suppressed basal TOP-GFP expression (figure 4C) and basal levels of nuclear axin-2 (figure 4D), both of which were rescued by addition of exogenous Wnt-3A. Wnt-3A mRNA was found to be expressed in freshly isolated crypts by RT-PCR and Wnt-3A ligand was immunolocalised to the stem cell region at the human colonic crypt-base (figure 4E).

TGFβ and BMP signalling pathway status in cultured human colonic crypts was assessed by phospho-SMAD immunofluorescence. A83–01 suppressed the TGFβ-induced increase in nuclear

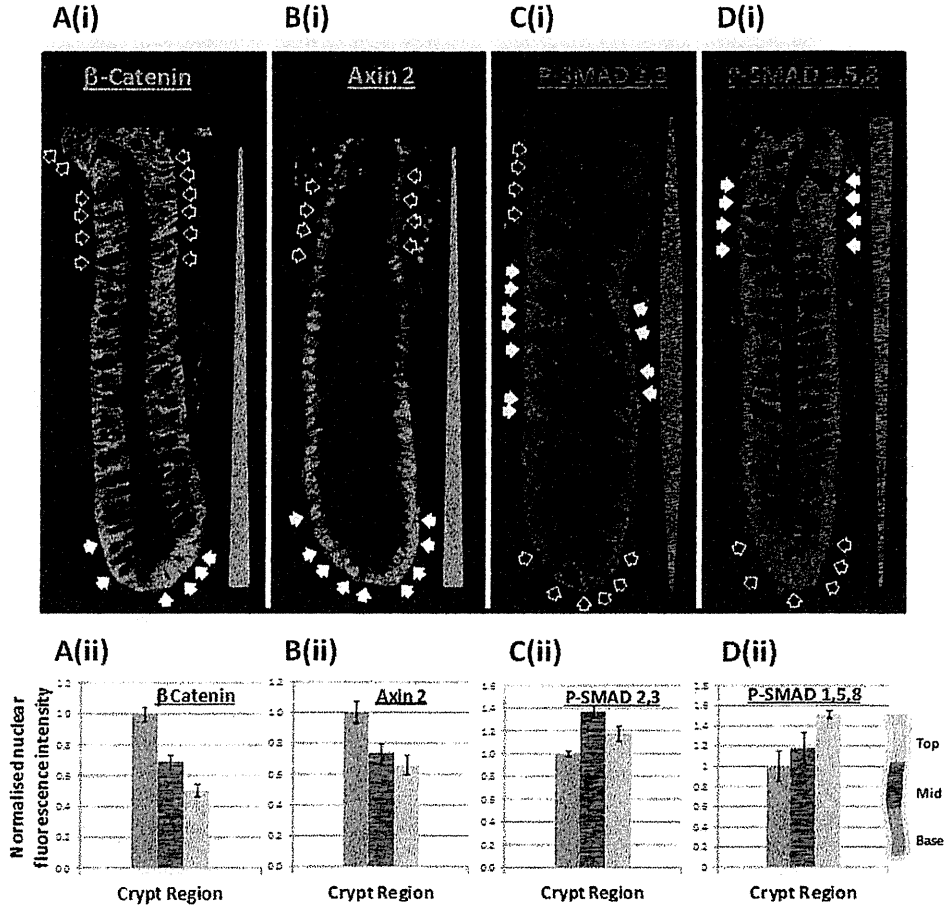

Figure 2 Wnt/β catenin and SMAD signalling profiles along the native human colonic crypt-axis. (Ai) Immunolabelling of total β catenin performed on native human colonic crypts reveals intense membrane and nuclear localisation at the colonic crypt-base. (Aii) The fluorescence intensity of nuclear β catenin predominates at the crypt-base and diminishes progressively towards the top of the crypt (Spearman Rank, r= −0.47, p<0.001). (B) A similar gradient exists for the immunofluorescence intensity of nuclear Axin-2 labelling (r=−0.48, p<0.001). Conversely, the immunofluorescence for nuclear phospho-SMAD 2,3 (C) predominates in the mid-crypt region, while nuclear phospho-SMAD 1,5,8 (D) exhibits a retrogradient that is more intense at the crypt opening (r=0.84, p<0.04). All values in each bar chart were normalised to the intensity value at the crypt-base. For each antibody, data were collated from n≥10 crypts microdissected from N≥3 patients. Filled arrowheads indicate intense nuclear labelling; open arrowheads mark nuclei of lower fluorescence intensity.

phospho-SMAD 2,3 levels (figure 5A), while noggin inhibited BMP stimulation of nuclear phospho-SMAD 1,5,8 levels (figure 5B). TGFβ and BMP inhibited the levels of nuclear axin-2, which was rescued by A83-01 (figure 5C) and noggin (figure 5D), respectively. It is noteworthy that A83-01 and noggin also augmented nuclear axin-2 levels in the absence of exogenous TGFβ or BMP ligand (figure 5C,D). These studies demonstrate that the Wnt signalling pathway in human colonic crypts is suppressed by TGFβ or BMP pathway activation. However, under optimal culture conditions, that is, Wnt stimulation in conjunction with BMP/ TGFβ suppression, the axin-2, p-SMAD 2,3 and p-SMAD 1,5,8 signalling gradients observed along the native human colonic crypt-axis (figure 2) were maintained ex vivo (see online supplementary figure S7). Also, analysis of marker genes for stem cells and differentiated crypt cell types indicated that the relative levels of gene expression in native crypts were similar to those placed in culture (see online supplementary figure S8). Taken together, these observations provided a good basis on which to investigate the relative influence of Wnt, BMP and TGFβ signalling pathways on human colonic crypt cell renewal.

Canonical Wnt signals support, and TGFβ/BMP signals inhibit, human colonic crypt stem/progenitor cell proliferation

Inspection of bright-field time-lapse movies (see online supplementary movies S2 and S3) revealed regular movements of cell nuclei and membranes in the proliferative zone of the crypt that were evocative of crypt cell mitoses. Accordingly, Wnt signals stimulated BrdU uptake and Ki67 labelling of cells located in the lower-half of human colonic crypts ex vivo (figure 6A,B). Inhibitors of Wnt signal transduction (DKK-1) and Wnt target gene activation (DN-TCF4 expression) abrogated Wnt-stimulation of human colonic crypt cell proliferation (figure 6A, B). Significantly, a population of LGR5$^+$/OLFM4$^+$ slender cells were interspersed between goblet-like cells within the cultured colonic crypt-base (figure 6C) in similar numbers found in the native crypt (*cf.* figures 1E and 6D,E). OLFM4 expression was inhibited by DKK-1 (figure 6D), as was *LGR5*-mRNA (not shown). An inhibitor of Wnt ligand secretion, IWP2, suppressed basal levels of LGR5 immunofluorescence and this was rescued by exogenous Wnt-3A (figure 6E,F); exogenous Wnt-3A also increased stem cell proliferation along the crypt-axis (figure 6G).

Human colonic crypts cultured over a period of at least 1 week continued to express markers of goblet (MUC-2), tuft (COX-1), enterocyte (FABP1) and enteroendocrine (chromogranin A) cell types (figure 6H) with a similar labelling pattern to that observed in native colonic crypts (see online supplementary figure S3). The ability of stem/progenitor cells to differentiate in culture was investigated by treating crypts with the notch inhibitor dibenzazepine. Crypt cells exhibited an increased number of MUC2$^+$ goblet cells (figure 6H,I)[20 21] and a decreased number of OLFM4$^+$ cells (figure 6J).[29]

The observations described thus far demonstrate that Wnt signals are prominent at the base of human colonic crypts and support intestinal stem cell biology and crypt cell proliferation. Given that TGFβ and BMP signals suppress Wnt signals (figure 5), it followed that they would also inhibit crypt cell proliferation. Accordingly, BrdU uptake was suppressed by omission of the BMP inhibitor noggin or the TGFβ inhibitor A83-01 (figure 7A,C). Exogenous BMP or TGFβ abolished BrdU uptake, which was rescued by noggin or A83-01, respectively (figure 7A,C). A

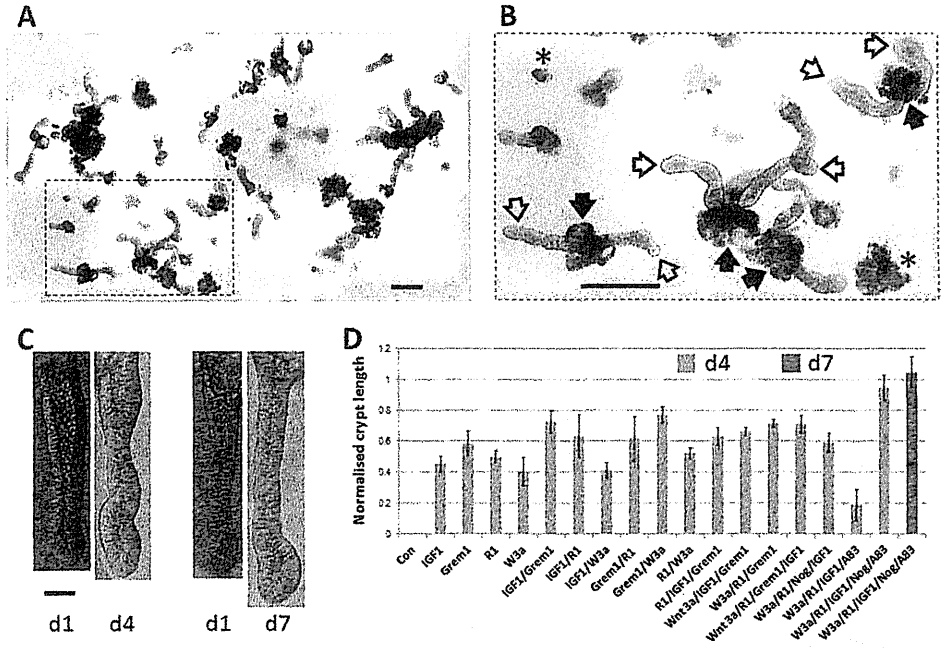

Figure 3 A combination of Wnt pathway activators and TGFβ/BMP pathway inhibitors is required for maintenance of cultured human colonic crypts ex vivo (A) Overview of human colonic crypts cultured within a Matrigel droplet under optimised conditions described in panel D; the bright field image was created by stitching together an array of 12 adjacent fields of view taken with a ×4 objective lens; scale bar=0.5 mm. (B) Enlargement of insert depicted in (A) representing a typical field of view (×4 objective lens); example crypt-base and shedding domains are denoted by open and closed arrowheads, respectively; *dead crypt fragments; scale bar=0.5 mm. (C) Example paired differential interference contrast images (×20 objective) of human colonic crypts cultured under optimised conditions for 0–4 and 0–7 days; d1=day 1, d4=day 4, d7=day 7; scale bar=100 μm. (D) Quantification of crypt length at day 4 or day 7 (with respect to the initial crypt length 4 h post-isolation, Day 0) following culture in the presence of the indicated combination of recombinant human growth factors, recombinant human BMP binding protein and/or small molecule ALK 4/5/7 inhibitor: IGF-1 (50 ng/mL), Gremlin-1 (200 ng/mL), Noggin (100 ng/mL), Wnt3A (100 ng/mL), R-Spondin-1 (500 ng/mL), A83-01 (0.5 μM); n≥6 crypts derived from N≥3 subjects.

neutralising pan-specific TGFβ antibody mimicked the effects of A83-01 (figure 7B) and a specific small molecule inhibitor of BMPR2/ALK2, DMH-1, reproduced the effect of noggin (figure 7D). In addition, activation of the BMP or TGFβ pathway abolished LGR5 expression (figure 7E).

Canonical Wnt signals combined with suppressed TGFβ/BMP pathways are permissive for tissue renewal ex vivo

The relative upward movement of crypt cells along the crypt-axis from the crypt-base was demonstrated by a classical BrdU pulse-chase approach (figure 8A). Inhibition of Wnt signalling with DKK-1 blocked the upward movement of BrdU pulse-labelled cells in the lower half of the crypt-axis into the upper-half of the crypt-axis (figure 8B). In addition to this relative migration of cells within the crypt frame of reference, absolute cell migration was also observed when crypts were cultured under suboptimal culture conditions (ie, reduced Wnt stimulation). Absolute crypt cell migration was associated with shortening of the crypt length (eg, see online supplementary figure S5), whereby the crypt-base migrated towards the crypt opening and crypt cells were shed from the surface (figure 8D). To explore the link between crypt cell proliferation and migration, crypts were cultured under conditions that imposed different levels of proliferation and were observed under time-lapse microscopy. Crypt length (figure 8Ci) and crypt cell proliferation followed a similar decreasing trend under culture conditions endowed with less proliferative potential (*cf.* figure 8Ci,Cii), but crypt cell migration rate stayed constant (figure 8Ciii). The average migration rate for crypts exhibiting a steady state length was 4.95±0.45 μm/h (n=20 crypts, N=4 patients). Cell shedding was localised to the upper crypt region as revealed by labelling of 'live' cultured crypts incubated with live/dead fluorophores, that is, calcein/propidium iodide (figure 8Di) and by immunolabelling fixed crypts for activated-caspase-3 (figure 8Dii). The accumulation of shed cells at the crypt opening was monitored in real time by observing discrete, intense bursts of red fluorescence associated with propidium iodide binding to cell nuclei following membrane rupture (figure 8Ciii and online supplementary movie S4). Thus, under these conditions, crypt cell proliferation in the lower half of the crypt is required to maintain a steady-state crypt cell population (eg, constant crypt length) by replenishing cells shed from the upper surface, but does not appear to drive (ie, mitotic pressure) crypt cell migration per se.

DISCUSSION

Intestinal tissue renewal is fundamental to long life and lifelong health. The processes by which the intestinal epithelium renews itself have been well described in the mouse, but the molecular and cellular mechanisms that govern tissue renewal in the human gut are less well understood. Central to gaining a more detailed understanding is the development of model systems for the native human intestinal epithelium. Ideally, these should recapitulate the processes of tissue renewal in health and disease. Another desirable requirement is that ex vivo human tissue models are amenable to bioimaging and functional genomic approaches. Complementary to the recent development of intestinal organoid culture systems, we have developed a culture model of near-native human colonic crypts. Presently, we have demonstrated a requirement for canonical Wnt signals and suppressed TGFβ/BMP pathways to support intestinal stem

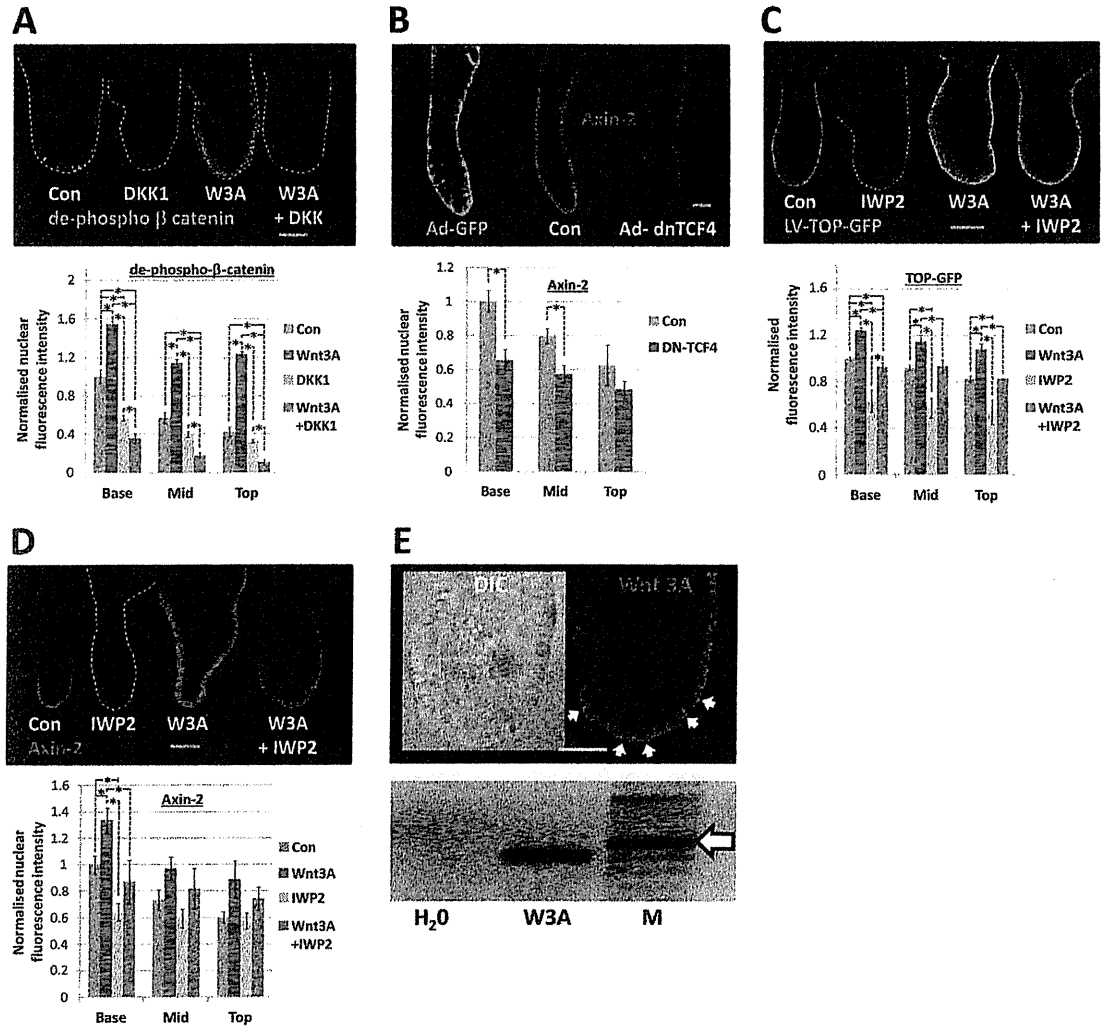

Figure 4 Exogenous and crypt-autonomous Wnt ligand promotes canonical Wnt/β catenin signals in cultured human colonic crypts. (A) Confocal images of dephospho β catenin immunolabelling following treatment with exogenous Wnt-3A (100 ng/mL, 30 min), in the presence or absence of Dikkopf-1 (DKK-1; 800 ng/mL); bar chart illustrates image analysis of nuclear immunofluorescence intensity. (B) Visualisation and analysis of nuclear Axin-2 3 days post-transduction with adenoviral GFP (Control: green Ad-GFP; red—Axin2) or dominant negative-TCF4. Effects of IWP2 (2 μM) on lentiviral (LV)-TOP-GFP expression (C) and nuclear axin-2 (D) immunofluorescence following 3 days culture. (E) Immunolabelling of human Wnt-3A (arrows indicate intense labelling basal membranes) and expression of Wnt-3A mRNA by RT-PCR using cDNA from freshly isolated human colonic crypts; expected Wnt 3A PCR product is 404 bp and the arrow denotes a 500 bp marker. All values in (A)–(D) bar charts were normalised to the control value in the crypt-base region. Control media: for A, C and D=IGF-1 (50 ng/mL)/Noggin (100 ng/mL)/R-spondin-1 (500 ng/mL); Wnt-3A (100 ng/mL) where indicated; for B=IGF-1 (50 ng/mL)/Noggin (100 ng/mL)/R-spondin-1 (500 ng/mL)/Wnt-3A (100 ng/mL). Statistical significance assessed by ANOVA followed by Tukey's post-hoc analysis; significant differences between pairs of mean values are indicated by linked dashed lines, *p<0.01; n≥4 crypts for each experimental group and the data are representative of at least three independent experiments in each case.

cell-driven tissue renewal in the human colon. Non-repressed TGFβ/BMP signals inhibited the canonical Wnt signalling pathway, intestinal stem cell marker expression and crypt cell proliferation, while unabated crypt cell migration and shedding resulted in the appearance of drastically shortened crypts and a compromised crypt cell population.

Intestinal stem cells play a central role in tissue renewal and a strategy to label these cells in situ was imperative. Lineage tracing,[8] propagation of self-renewing intestinal organoids[27] and transplantation[22] assays have defined LGR5 as a marker of proliferative intestinal stem cells. Characterisation of the mouse small intestinal stem cell transcriptome identified a number of highly enriched genes including OLFM4,[30] which, although not expressed in the mouse colon, was also enriched in human colonic stem cells.[21 31] The current study used confocal imaging of whole-mounted intact human colonic crypts to visualise double labelling of OLFM4 protein and either LGR5 protein or LGR5-mRNA at subcellular resolution. We identified a number of $LGR5^{+}/OLFM4^{+}$ slender cells at the base of human colonic crypts, interspersed between goblet-like cells. This is reminiscent of the case for LGR5-GFP positive cells in the mouse colon.[32] A subpopulation of $LGR5^{+}/OLFM4^{+}$ cells existed that were more intensely labelled with LGR5 protein or mRNA (figure 1C,D). By analogy with sorting of single $LGR5^{GFP\text{-}Hi}$ cells from the mouse intestine[32] and $EPHB2^{Hi}$ (a surrogate marker for LGR5-positive cells) cells from the human colon,[21] it is likely that immunolabelling of $LGR5^{Hi}/OLFM4^{+}$ cells indicate the human intestinal stem cells proper and that $LGR5^{Lo}/OLFM4^{+}$ are progenitors. Indeed, OLFM4 mRNA expression has been shown to extend beyond $LGF5^{Hi}$ cells.[26 33] It is also noteworthy that recent observations of the mouse intestine

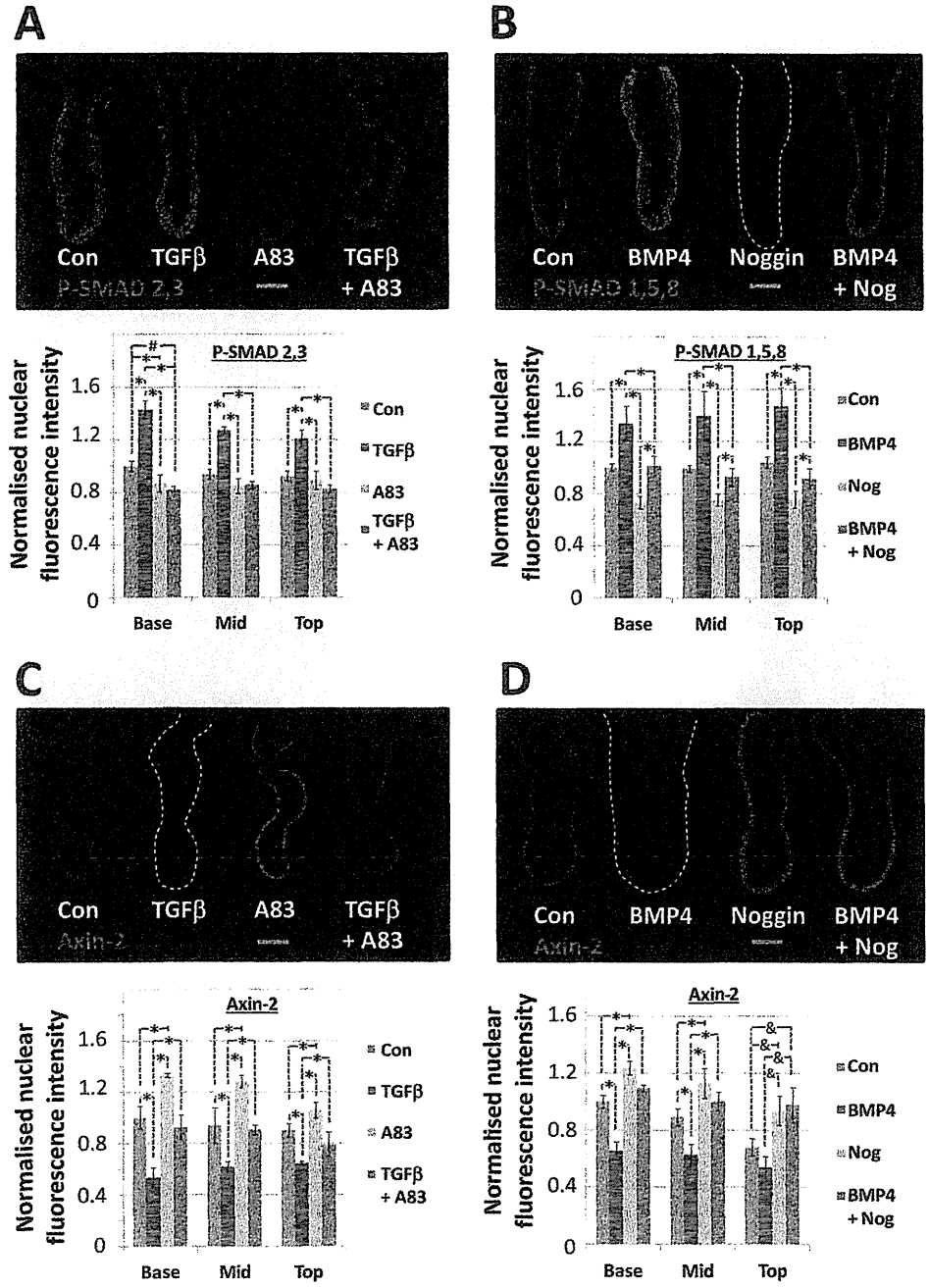

Figure 5 TGFβ and BMP pathway activation inhibits canonical Wnt signalling along the cultured human colonic crypt-axis. (A) Confocal images of phospho-SMAD2,3 immunolabelling following treatment with TGFβ (20 ng/mL, 2 days), in the presence or absence of A83-01 (0.5 μM); bar chart illustrates image analysis of nuclear immunofluorescence intensity. (B) Effects of BMP (100 ng/mL, 2 days) and/or noggin (100 ng/mL) on nuclear phospho-SMAD1,5,8 immunofluorescence intensity levels. (C) TGFβ and (D) BMP suppression of nuclear Axin-2 immunofluorescence, and rescue by pretreatment with noggin or A83-01, respectively. All values in (A–D) were normalised to the control value in the crypt-base region. Culture conditions: (A and C)—IGF-1 (50 ng/mL)/R-spondin-1 (500 ng/mL)/Wnt-3A (100 ng/mL)/Noggin(100 ng/mL) and TGFβ (20 ng/mL) and/or A83-01 (0.5 μM) where indicated; (B and D)—IGF-1 (50 ng/mL)/R-spondin-1 (500 ng/mL)/Wnt 3A (100 ng/mL)/A83-01 (0.5 μM) and BMP (100 ng/mL) and/or noggin (100 ng/mL) where indicated. Significant differences were assessed by ANOVA followed by Tukey's post-hoc analysis; significant differences between pairs of mean values are indicated by linked dashed lines; $^{\#}p<0.01$, $^{*}p<0.02$, $^{\&}p<0.05$; $n\geq4$ crypts for each experimental group and the data are representative of at least three independent experiments in each case. Scale bars=75 μm.

point to increased plasticity of crypt progenitor cells in that they can dedifferentiate into intestinal stem cells following injury.[34] In this respect, it will be fascinating to determine the precise relationship between $LGR5^{Hi}/OLFM4^{+}$ cells, $LGR5^{Lo}/OLFM4^{+}$ cells and stem cell potential following injury, and with respect to ageing and cancer risk.[35]

A functional role for morphogen gradients in conferring a crypt stem/progenitor phenotype was indicated by distinct profiles of signal pathway activation along the crypt-axis (figure 2). Substituting EGF with IGF-1 restrained the formation of multiple buds that is associated with mass expansion of intestinal stem cells in organoid culture.[20 21] These modified conditions